AD-A150 696 RESEARCH DIRECTED ADVANCED HIGH TEMPERATURE COATING SYSTEM BEYOND CURRENT..(U) PITTSBURGH UNIV PA DEPT OF METALLURGICAL AND MATERIALS ENGINE.. A ASHARY ET AL. 1/1

UNCLASSIFIED DEC 84 AFOSR-TR-84-1278 AFOSR-80-0089 F/G 11/6 NL

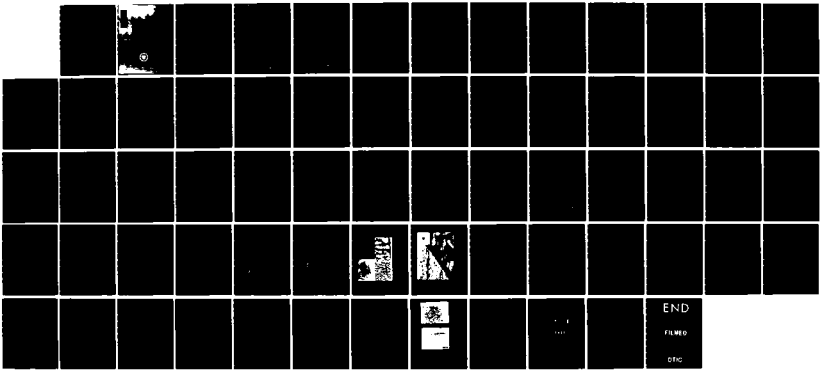

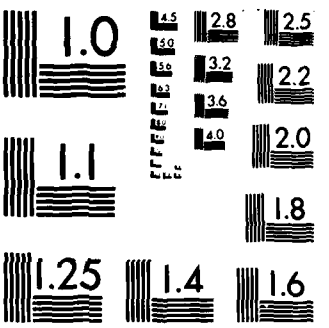

3

RESEARCH DIRECTED TO ADVANCED HIGH TEMPERATURE COATING SYSTEM BEYOND CURRENT STATE-OF-THE ART SYSTEMS

METALLURGICAL AND MATERIALS ENGINEERING

University of Pittsburgh
Pittsburgh, Pennsylvania 15261

"Original contains color plates: All DTIC reproductions will be in black and white."

(3)

RESEARCH DIRECTED TO ADVANCED HIGH TEMPERATURE COATING SYSTEM BEYOND CURRENT STATE-OF-THE ART SYSTEMS

FOURTH ANNUAL REPORT
ON
CONTRACT NO. 80-0089
(Period Covered January 1, 1983-January 1, 1984)

SUBMITTED TO
AFOSR

By

A. Ashary, G.H. Meier and F.S. Pettit
Department of Metallurgical and Materials Engineering
University of Pittsburgyh
Pittsburgh, PA. 15261

UNCLASSIFIED

SECURITY CLASSIFICATION OF THIS PAGE (When Data Entered)

REPORT DOCUMENTATION PAGE	READ INSTRUCTIONS BEFORE COMPLETING FORM
1. REPORT NUMBER: AFOSR-TR- 84-1278	2. GOVT ACCESSION NO.: AD-A150696
	3. RECIPIENT'S CATALOG NUMBER
4. TITLE (and Subtitle): RESEARCH DIRECTED TO ADVANCED HIGH TEMPERATURE COATING SYSTEM BEYOND CURRENT STATE-OF-THE ART SYSTEMS	5. TYPE OF REPORT & PERIOD COVERED: ANNUAL 1 JAN 83 to 1 JAN 84
	6. PERFORMING ORG. REPORT NUMBER
7. AUTHOR(s): A. Ashary, G. H. Meier and F. S. Pettit	8. CONTRACT OR GRANT NUMBER(s): AFOSR-80-0089
9. PERFORMING ORGANIZATION NAME AND ADDRESS: UNIVERSITY OF PITTSBURGH, Dept of Metallurgical & Materials Engineering, Pittsburgh, PA 15261	10. PROGRAM ELEMENT, PROJECT, TASK AREA & WORK UNIT NUMBERS: 61102F, 2306/A2
11. CONTROLLING OFFICE NAME AND ADDRESS: AFOSR/NE, Bldg 410, Bolling AFB DC 20332-6448	12. REPORT DATE: December 1984
	13. NUMBER OF PAGES: 58
14. MONITORING AGENCY NAME & ADDRESS(if different from Controlling Office)	15. SECURITY CLASS. (of this report): Unclassified
	15a. DECLASSIFICATION/DOWNGRADING SCHEDULE

16. DISTRIBUTION STATEMENT (of this Report)

Approved for public release; distribution unlimited.

17. DISTRIBUTION STATEMENT (of the abstract entered in Block 20, if different from Report)

18. SUPPLEMENTARY NOTES

"Original contains color plates: All DTIC reproductions will be in black and white"

19. KEY WORDS (Continue on reverse side if necessary and identify by block number)

Silica Scales, Isothermal Oxidation, Cyclic Oxidation, Acoustic Emission Experiments.

20. ABSTRACT (Continue on reverse side if necessary and identify by block number)

Alloy systems have been investigated to determine the reaction product barriers that can be used to provide optimum resistance to high temperature oxidation. The reaction product barriers which can be used are -Al(2)0(3), Cr(2)0(3) and Si0(2) with the use Cr(2)0(3) being restricted to below about 1000C due to formation of volatile products.

The oxidation of nickel-silicon alloys has been studied over the internal 900-1100C. Compositions of 20-22.5 Si have been found to form protective, adherent scales of Si0(2). The oxidation resistance of these alloys appears to be comparable

DD FORM 1 JAN 73 1473 EDITION OF 1 NOV 65 IS OBSOLETE

SECURITY CLASSIFICATION OF THIS PAGE (When Data Entered) UNCLASSIFIED

to the most oxidation resistant alumina-forming alloys.

The cracking and spalling of Al(2)0(3) scales from alloys has been described by using acoustic emission analyses to conventional analytical techniques. It has been found that acoustic emission counts can be used to indicate the damage in alumina scales.

A mechanism to describe the oxidation of oxygen active elements in alloys has been developed. The effects of yttrium and hafrium on the adherence of Al(2)0(3) to NiCrAl and CoCrAl alloys has been compared. It is shown that the concentration of the oxygen active elements and the substrate composition are significant factors affecting oxide scale adherence.

TABLE OF CONTENTS

ABSTRACT

Alloy systems have been investigated to determine the reaction product barriers that can be used to provide optimum resistance to high temperature oxidation. The reaction product barriers which can be used are -Al_2O_3, Cr_2O_3 and SiO_2 with the use Cr_2O_3 being restricted to below about 1000°C due to formation of volatile products.

The oxidation of nickel-silicon alloys has been studied over the internal 900-1100°C. Compositions of 20-22.5 Si have been found to form protective, adherent scales of SiO_2. The oxidation resistance of these alloys appears to be comparable to the most oxidation resistant alumina-forming alloys.

The cracking and spalling of Al_2O_3 scales from alloys has been described by usng acoustic emission analyses to conventional analytical techniques. It has been found that acoustic emission counts can be used to indicate the damage in alumina scales.

A mechanism to describe the oxidation of oxygen active elements in alloys has been developed. The effects of yttrium and hafrium on the adherence of Al_2O_3 to NiCrAl and CoCrAl alloys has been compared. It is shown that the concentration of the oxygen active elements and the substrate composition are significant factors affecting oxide scale adherence. Originator supplied key words include:

A1

INTRODUCTION

This program is concerned with defining coatings compositions, structures and surface treatments which can be used to obtain new systems possessing superior high temperature oxidation resistance compared to the current state-of-the-art MCrAlY systems and diffusion aluminide coatings. The approach which is being used consists of attempting to obtain reaction product barriers with improved protective properties compared to those formed on state-of-the-art systems.

A number of oxide systems have been examined in this program and their protectiveness as reaction product barriers compared (e.g. -Al $_2O_3$, Cr_2O_3, SiO_2, MgO, BeO). It has been concluded that only alumina (-Al $_2O_3$) and silica (SiO_2) have potential for use to develop improved systems.

The further investigation of alumina and silica scales has been pursued by using a variety of conventional tests, in particular, isothermal and cyclic oxidation where specimens after exposure have been examined by using optical and scanning metallography. From the onset of these investigations, however, it was apparent that these conventional testing techniques were not an adequate means to compare the protectiveness of these scales. Hence several new test procedures have been examined and used to more effectively study and compare the protective properties of alumina and silica. These tests have involved the development of procedures to measure the load to pull such scales from the surfaces of alloys, and the use of acoustic emission measurements to describe the cracking and spalling in the scales upon cooling from the test temperature. The significant results that were obtained upon the

conclusion of the third year of this program are discussed in the following sections.

USE OF SILICA SCALES AS PROTECTIVE BARRIERS

Silica scales formed on nickel-silicon alloys (e.g. Ni-20Si, Ni-22SI)* were found to have growth rates substantially less than those for alumina and chromia scales formed under similar conditions, Figure 1. Such scales, based upon their growth rates, appear to have potential for use as reaction product barriers formed on coatings on high temperature alloys in place of the alumina scales which are formed upon the current state-of-the-art MCrAlY coatings. During the fourth year of this program it was attempted to characterize these silica scales in more detail to define structures (amorphous versus crystalline) that are critical for inproved oxidation resistance and to determine their capability to resist cracking and spalling under the influence of thermally induced stresses. Special emphasis was placed upon defining the compositions and structures of alloys upon which the most protective silica scales were formed.

DEVELOPMENT OF NEW TESTING TECHNIQUES

A problem of very significant magnitude which is encountered in attempting to study and compare the protectiveness of reaction product barriers on alloys is the lack of adequate test procedures to measure oxide scale adherence. In this program some new techniques have been examined and utilized. Two tests which appeared to have merit are, one whereby the load required to pull scales from their substrates was measured, and another that uses acoustic emission measurements to

---

*All compositions are given in weight percent.

attempt to characterize the cracking and spalling processes in oxide scales formed upon alloys. The technique to measure the load required to pull scales from their substrates was not as effective as desired [1] because for very adherent scales, failure occurred in the epoxy used to attach the stud to the oxide scale surface. In addition the reproducibility of results obtained from this test were not sufficient to permit the required comparisons. The use of acoustic emission measurements, on the other hand, did produce very meaningful results as discussed in previous publications[1,2]. In particular the cumulative acoustic emission counts were found to be a measure of the damage in the scale, Figure 2. It also appeared that the amplitude of the counts could be used to characterize specific details of the damage but more work was necessary to conclusively establish this result.

COMPARISON CYCLIC OXIDATION ACTIVE ELEMENT EFFECTS OF Al_2O_3 SCALE ADHESION

Using cyclic oxidation tests and acoustic emission measurements, it was found that the adherence of Al_2O_3 scales were affected by the type and concentration of oxygen active elements. Moreover the base alloy composition (e.g. nickel-versus cobalt-base) also was found to affect oxide adherence.

The fourth year of this program was used to attempt to determine what elements and concentrations were mose effective in optimizing the adherence of α-Al_2O_3 on nickel-and cobalt-base alloys. An important part of this effort was to develop a model for the oxidation of oxygen active elements in such alloys.

EXPERIMENTAL

The experimental techniques used in this program have been described in the third annual report. They will only be briefly discussed in the current report.

SPECIMEN PREPARATION

Alloys were prepared by tungsten arc melting under an argon atmosphere and drop casting into molds. The dimensions of the molds were 150 mm X 25 mm X 9 mm or 150 mm X 160 mm dia. The ingots were homogenized by heating in argon for 100 hrs. at 1150°C. Specimen shapes were either 12 mm X 9 mm X 2 mm or 16 mm dia. X 2 mm. The specimens were polished through 600 grit and and ultrasonically cleaned in alcohol prior to oxidation testing.

ISOTHERMAL OXIDATION

Isothermal oxidation testing was performed by using a Cahn Microbalance and a furnace assembly consisting of a quartz reaction tube and appropriate glassware to provide a gas tight system. The specimens were oxidized in flowing or static air and weight changes were measured continuously as a function of time.

CYCLIC OXIDATION

Long term cyclic oxidation testing was carried out by exposing specimens in laboratory air in an apparatus which automatically removed the specimens from the furnace and reinserted them at selected time intervals. Each cycle consisted of 45 minut4es isothermal oxidation followed by cooling for 15 minutes outside the furnace. The specimens were weighed after every 20 to 30 hours exposure time.

EXAMINATION OF EXPOSED SPECIMENS

Specimens were examined routinely by using optical metallography, scanning electron microscopy and x-ray diffraction. Some specimens were occasionally examined by using scanning auger microscopy.

ACOUSTIC EMISSION EXPERIMENTS

The acoustic emission measurements were made by using a platinum wave guide to transmit the signals from the specimens to a piezoelectric transducer. The acoustic emission apparatus used was a Dunegan-Endevco-3000 series detection system. Schematic diagrams are presented in Figure 3 and 4. The signal, shown schematically in Figure 5 consists of a damped sinusoidal wave with a frequency corresponding approximately to the resonant frequency of the transducer. A given acoustic emission event within the specimen produces several counts associated with the number of times the signal crosses the threshold voltage, V_t in "ringing down" to a voltage below the trigger level. Three counts would result from the signal shown in Figure 5. Larger events produce more counts in ringing down so the number of counts is a measure of the energy released in an event.

Specimens were usually oxidized for 24 hours in air at 1000, 1050, or 1100°C and then cooled either in the furnace or outside in air. The specimen temperature as a function of time was obtained from a thermocouple welded to a dummy specimen. Acoustic emission counts were recorded both during isothermal oxidation and the cooling periods. However, during cooling a total signal amplification of 80 dB was used while during isothermal oxidation a 90 dB grain was used since the acoustic emission activity was weak during the latter.

RESULTS AND DISCUSSION

In this section the results obtained during the fourth year of the program are presented and discussed. The results have been divided into the three areas of emphasis, namely, silica scales, acoustic emission analyses, and the effects of oxygen active elements on Al_2O_3 adherence.

SILICA SCALES

Alloys and coatings for high temperature applications generally obtain oxidation resistance by the selective oxidation of Cr or Al to form protective surface films of Cr_2O_3 or Al_2O_3. As a result, the formation of Cr_2O_3 and Al_2O_3 have been extensively studied (e.g. refs. 3 and 4). The selective oxidation of Si to form SiO_2 films has not been investigated in great detail but appears to offer great potential as another means of protecting high temperature alloys and coatings. In this section the literature on the formation of SiO_2 on pure Si (generated mainly in studies of semiconductor device fabrication) and on the oxidation of alloys and ceramics which form protective oxides which are rich in Si will be briefly reviewed. The results of the experimental study on the high temperature oxidation of binary Ni-Si alloys will then be described.

Oxidation of Si

The oxidation of Si to form an amorphous SiO_2 layer is generally assumed to follow what ore termed "linear-parabolic kinetics". This growth law introduced by Deal and Grove[5] may be written:

$$x^2 + Ax = Bt \qquad (1)$$

some values obtained for NiCrAl alloys with Y and Hf are compared. These results will be discussed in a later section.

THE OXIDATION OF OXYGEN ACTIVE ELEMENTS AND EFFECTS ON ALUMINA ADHERENCE

While the effects of oxygen active elements have been of interest for over fifty years, very little work has been done on describing how these elements oxidize. Giggins and Pettit [27] and Whittle and coworkers [28] have shown that the pegs of oxygen active elements become coated with alumina when alumina forming alloys contain oxygen active elements. In the following the oxidation of oxygen active elements is discussed and then the effects produced by several oxygen active elements on alumina adhesion is described.

Oxidation of Oxygen Acctive Elements in Alloys

When oxygen active elements are added to alloys to influence oxide scale adherence the concentrations of these elements usually is between 0.05 and 2.0 weight percent. The elements withlow solubility such as yttrium are on the low side of this range and the elements with high solubility are on the high side of this range. hence in discussing oxygen active element oxidation it seems reasonable to consider alloys with concentrations in this range.

A characteristic feature of this oxidation, for Al_2O_3-forming alloys, that is often observed is the development of protrusions of pegs which extend from the extermal oxide scale into the alloy. When the element has a high solubility the number of protrusions is usually high,

amplitudes were also obtained for the NiCrAlY alloy. A diagram comparing peak amplitudes of NiCrAl 1.2Y, NiCrAl.07Y and NiCrAl.-Hf is presented in Figure 25. The trend is for more events at all amplitudes in the sequence NiCrAl-1.2Y, NiCrAl-Hf, NicrAl10.071Y. The higher peak amplitudes also follow this trend to a limited extent.

The results obtained from cyclic oxidation of these alloys are presented in Figure 26. It is evident that the two alloys with the least spalling are CoCrAlY and CoCrAlHF followed by sequentially NiCrAl-0.71Y, NiCrAl-.0084 and NiCrAl-1.0Hf. These results suggest that the number of events increase as the amount of oxide scale cracking and spalling increases. However, it also appears that the highest amplitude events may be associated with the spalling events since higher peak amplitudes were obtained when rather severe spalling of the scales was evident.

The observation that higher peak amplitudes are obtained when spalling of oxides is commonplace has also been o bserved for NiCrAlCe and NiCrAlZr, Figure 27. Such results suggest that peak amplitude analyses may be used to characterize or differentiate between cracking and spalling. Future work will be directed to further examine peak amplitudes to determine if they can be used as a means of analyzing coatings in regard to the useful life remaining.

If the counts for spalling and for cracking can be differentiated, it can be attempted to give counts for spalling in terms of counts per unit area. When the spalling occurs along the alloy- oxide interface, such calculations permit a comparison of the influence of the oxygen active elements on the bonding between alumina scales and alloys. In Table I

taken as fracture within the oxide scale more or less perpendicular to the specimen surface and spalling is fracture parallel to the specimen surface usually along the oxide scale-alloy interface. The number of acoustic emission counts is proportional to the energy released upon cracking and spalling of the oxide scale. The acoustic emission data can be also plotted to attempt to relate different events to their peak amplitudes. The experimental equipment, in principle, is capable of determining the peak amplitude associated with the ring down of a given event. In practice a problem arises due to superposition of waves from different events. Superposition effects can be minimized by making the event analysis time large. During this time new imput will not be accepted until analysis of a given ring down is complete. The problem with this latter procedure is that some data will not be accepted and hence lost. The problems of superposition are not easily resolved. In the present investigation it was decided to select an analysis time and to attempt to determine if changes should be made after an initial analysis of the data.

In Figures 18-22 amplitude distribution obtained upon cooling oxidized specimens after 24 hours of oxidation at 1100^{o}C are presented for six consecutive oxidation cycles. These data are best compared by superposition of the data for different alloys. The results obtained for the two CoCrAl specimens are presented in Figure 23. No significant difference is evident for CoCrAlY and CoCrAlHf for any of the six cycles. In Figure 24 the data for NiCrAl10.071Y is compared to the CoCrAlY alloy. In general the number of events at all amplitudes is greater for NiCrAl.07Y alloy. Moreoever significant higher peak

kinetics, and that the Ni_2SiO_4 has formed by reaction of transient NiO with the SiO_2. More work is needed to characterize the oxidation products at higher temperatures and longer times.

Figures 15 through 17 show the cyclic oxidation weight changes for the Ni-Si alloys at 900, 1000, and 1100°C. It is seen that the alloys containing 5, 7.5, 10, 15, and 17.5 wt. pct. Si exhibit significant weight losses due to scale spallation whereas the Ni-20 Si and Ni-22.5 Si alloys show little degradation. The thin SiO_2 scales on these alloys were observed to be extremely adherent. The Ni-12.5 Si alloy showed rather interesting behavior in that the alloy initially lost weight (for approx. the first 100 cycles) and then showed a negligible weight change for the remainder of the exposures. The cause of this behavior is being investigated further.

In summary, the alloys in the Ni-Si system undergo a number of interesting oxidation phenomena. Those alloys containing 20-22.5 wt. pct. Si exhibit extremely slow rates of isothermal oxidation and are resistant to thermal cycling. It is believed that these alloys may form the basis for coatings which are improvements over the current MCrAlY and aluminide coatings.

ACOUSTIC EMISSION ANALYSES

During the fourth year of this program work was performed to determine if acoustic emission could be used to characterize the nature of the oxide scale damage. Previous results [1,2] had shown the number of counts correlated well with the cracking and spalling of oxide scales as determined by cyclic oxidation tests. An important question is how much of this damage is cracking and how much is spalling? Cracking is

in extremely slow oxidation rates. The cause of the anomolous behavior of the Ni-15 Si and Ni-17.5 Si is not understood and is being investigated further.

The oxidation data for Ni-5 Si at 1100°C are included in Figure 8 and are seen to be in good agreement with those of Cocking et al [24]. The data for Ni-5 Si and Ni-10 Si at 1000°C are included in Figure 9 for comparison with those of Kerr and Simkovich[25]. It is seen that the alloys in this study oxidize more slowly than their counterparts in the work of Kerr and Simkovich. This is due to the factor of five higher P_{O_2} (O_2 vs air) used by Kerr and Simkovich which would result in faster growth rates of both NiO and SiO_2.

As pointed out earlier and shown in Figure 1 the oxidation rates of Ni-20 Si and Ni-22, 5 Si are slower than those for Al_2O_3-forming alloys. Figure 13 shows the surface of an electropolished specimen of Ni-20 Si and indicates the Si concentrations of the constitutents.[26]. The smooth-appearing regions correspond to the δ (Ni_2Si) phase while the grainy appearing region corresponds to $\delta + \varepsilon$(Ni_3Si_2) formed by eutectoid decomposition of the high temperature O-phase. Figure 14 shows a transmission electron micrograph of the oxide formed over the two phases after one hour at 950°C.[26]. The light area is oxide formed over the $\delta + \varepsilon$ region and is indicated by selected area diffraction and auger analysis to be amorphous SiO_2. The dark oxide has formed over the δ-phase and is indicated by the superposed selected area diffraction pattern to be Ni_2SiO_4. The dark islands over the $\delta + \varepsilon$ region were also found to be Ni_2SiO_4. It, therefore, appears that the alloy is covered by an amorphous SiO_2 layer, which is responsible for the slow oxidation

these coatings is usually complex and difficult to characterize in terms of mechanisms.

Two studies[24,25] have been published on the oxidation of alloys in the binary Ni-Si system. Cocking et al[24] studied the oxidation of solid solution alloys containing 0 to 5.2 wt. pct. Si in air at temperatures between 900 and 1200°C. The weight change versus time data at 1100°C are plotted in Figure 8. Increasing Si concentrations are seen to result in slower oxidation rates. The oxidation products were observed to contain NiO, SiO_2, and Ni_2SiO_4. Kerr and Simkovich[25] studied the oxidation of alloys containing 0 to 10.1 wt. pct Si at 1000°C in one atm of O_2. Small additions of Si up to 1 wt. pct were observed to accelerate the oxidation rate which was explained as a doping effect of Si in the NiO scale. Oxidation rates continually decreased with increasing Si concentration above 2.5 wt. pct. Si. The weight change vs. time data for three of the alloys are plotted in Figure 9. The oxidation products responsible for the slower oxidation rates were not clearly identified.

Results of the Current Study

In the present studies Ni-Si alloys containing 5 to 22.5 wt. pct Si have been oxidized in air at temperatures between 900 and 1100°C. Figures 10 through 12 present the weight change versus time data for these alloys at 900, 1000, and 1100°C. The oxidation rates at all three temperature are seen to decrease with increasing Si concentration from 5 to 12.5 wt. pct. However, the oxidation rates for alloys containing 15 and 17.5 wt. pct. Si are observed to oxidize at rates faster than Ni-7.5 Si. Increasing the Si concentration further to 20 or 22.5 wt. pct. results

A more rigorous treatment of the problem (17) yields a slightly different expression for the critical oxygen pressure

$$P_{O_2}(\text{crit}) = \tfrac{1}{2} \left(\frac{P_{SiO}}{P_{O_2}} \right)^{\frac{1}{2}} P_{SiO}(\text{eq.}) \qquad (22)$$

Gulbransen et al[19] have tested Wagner's prediction by oxidizing Si over a range of temperatures and oxygen pressures and found good agreement. The rate of Si consumption was approximately 300 times faster for oxygen pressures below P_{O_2}(crit) than those above it. Interestingly, this is a phenomenon which is rare in high temperature oxidation but rather more common in aqueous corrosion, i.e. the rate of reaction being slower at higher driving forces (passive) than lower driving forces (active).

Similar active-passive behavior has also been observed for Si-base ceramics such as SiC and Si_3N_4 during oxidation at low oxygen pressures[20-22].

Oxidation of SiO_2-Forming Alloys

The oxidation of Si-containing coatings has been reviewed recently by Grinling and Bauer[23]. Most of the work in this area has involved silicide coatings on refractory metals and superalloys in which the coatings are formed by Si-diffusion processes. The oxidation of

where p_{SiO} is the pressure of SiO at the Si surface and P_{O_2} is the oxygen pressure in the bulk gas. Under steady state conditions, the net transport rate of oxygen atoms must vanish. Therefore

$$2 J_{O_2} = J_{SiO} \tag{17}$$

which upon substitution of equations 15 and 16 and assuming $D_{SiO} \sim$ yields,

$$P_{SiO} = 2 \bar{P}_{O_2} \tag{18}$$

If the equilibrium SiO pressure from the reaction

$$\tfrac{1}{2} \text{ Si (S or l)} + \tfrac{1}{2} \text{ SiO}_2 \text{ (S)} = \text{SiO (g)} \tag{19}$$

is greater than the SiO pressure in equation (18, the Si surface will remain bare and Si will be continually consumed. Therefore, there is a critical oxygen pressure

$$P_{O_2} \text{ (crit)} \simeq \tfrac{1}{2} P_{SiO} \text{ (eq.)} \tag{20}$$

below which 'active' oxidation will occur and the rate of metal consumption will be controlled by the SiO flux away from the surface

$$J_{SiO} = \frac{2 P_{O_2} D_{O_2}}{\delta RT} \tag{21}$$

the diffusion coefficient of oxidant in the inner region of the SiO_2 layer due to compressive stresses[15]. These stresses are partially relieved by viscous flow below 950°C, giving rise to the variation in activation energy, and are completely relieved above 950°C. Generation of compressive stresses in the oxide have also been used to explain the reduced oxide thickness formed over step-edges on nonplanar Si surfaces[16].

The oxidation of Si can be markedly influenced by oxide vapor species at low oxygen pressures. The reason for this may be seen from the volatile species diagram for the Si-O system in Figure 7. A significant pressure of SiO is seen near the dissociation pressure of SiO_2(s) and Si(s) at oxygen pressures near the dissociation pressure of SiO_2. This can result in a rapid flux of SiO away from the specimen surface and the subsequent formation of a non-protective SiO_2 smoke. The formation of the SiO_2 as a smoke rather than as a continuous layer allows continued rapid reaction.

Wagner[17,18] has analysed the conditions under which this 'active' oxidation occurs. A simplified version[18] of this analysis follows. The fluxes of O_2 and SiO across a hydrodynamic boundary layer, taken to be the same thickness, d, for both species, are given by

$$J_{O_2} = \frac{p_{O_2} D_{O_2}}{\delta RT} \tag{15}$$

and

$$J_{SiO} = \frac{p_{SiO} D_{SiO}}{\delta RT} \tag{16}$$

through)[10,11] and, alternatively, to the formation of channels formed perpendicular to the specimen surface by localized structural ordering of the SiO2[9]. Pores have been reported in SiO_2 films grown on Si based on transmission electron microscopy results[12] but the exact nature of the paths for oxidant transport is not yet resolved.

The linear rate constant, k_l, is observed to depend on P_{O_2} raised to a power, m, which is usually between 0.6 and 0.8 rather than linearly on P_{O_2}as would be expected from Eqn. (3).[13]This requires the expression for the interface reaction to be written as

$$R = k N_1^m \qquad (14)$$

so that the overall kinetics cannot be strictly "linear parabolic". Hu[13] has derived a more complex rate law taking this into account and has analyzed the reaction at the Si/SiO_2 interface as being controlled by chemisorption of oxidant.

The oxidation of Si by water vapor is much faster than in dry oxygen with both k_p and k_l being increased. When oxidation is carried out in pure water vapor k_p ad k_l are found to vary linearly with the partial pressure of water vapor.[14] The transport of oxidant is proposed to occur by the ambipolar diffusion of hydronium (G_3O^+) and hydroxl (OH^-) ions[14].

The growth of SiO_2 on Si has also been reported to be influenced by growth stresses generated by the formation of new oxide at the Si/SiO_2 interface. The activation energy associated with k_p is found to be independent of temperature above about 950°C but to vary with temperature below 950°C. This has been explained as a reduction of

and

$$k_1 = 3.71 \times 10^6 \exp\left(-\frac{2.0\ ev}{kt}\right) \frac{\mu m}{h} \text{ for } (100)Si$$

when the oxidation is carried out in one atm of dry oxygen.

There is general agreement that amorphous SiO_2 grows on Si by the inward transport of oxidant. This is based on observations that (i) $kp P_{O_2}$, (ii) the activation energy for oxygen diffusion and oxidation are virtually equal at high temperatures and (iii) experiments in which the oxidizing gas is switched after some exposure time from 0^{16} to 0^{18} results in nearly all of the 0^{18} being concentrated at the Si/SiO_2 omterface [7]. However, there is some question regarding the particular oxidizing species which is transported and considerable controversy regarding the nature of the transport path through the oxide. Kroger[8] has recently reviewed the literature on the defect structure of SiO_2 and concludes that the major species transported are charged oxygen interstitials, $O_{2,i}$ and $O_{2,i}$, but uncharged O_2 is probably not much slower. The transport by charged species is not consistent with $kp \propto P_{O_2}$ as pointed out by Kroger[8].

The rate of growth of amorphous SiO_2 on Si occurs with rates several times faster than those calculated from the diffusion coefficient of oxygen in vitreous SiO_2[9], thus indicating the presence of short-curcuit paths through the oxide. These paths have been proposed to be "micropores" extending through the oxide (or nearly

which identifies the constants in Eqn (1) as $A = \frac{2D}{k}$

and

$$B = \frac{2DN_o}{n}$$

For short times and low temperatures

$$x = \frac{B}{A} t \qquad (12)$$

and for long times and higher temperatures

$$x = B^{\frac{1}{2}} t^{\frac{1}{2}} \qquad (13)$$

so that B/A is referred to as the "linear rate constant, k_l and B as the "parabolic rate constant, k_p".

Much of the work on the oxidation of Si has concentrated on the effects of temperature, oxygen partial pressure, crystallographic orientation, and water vapor in the oxidizing gas on the linear and parabolic rate constants. The magnitudes of these constants are [6]

$$k_p = 7.72 \times 10^2 \exp\left(-\frac{1.23ev}{kT}\right) \frac{\mu m^2}{h}$$

$$k_l = 6.23 \times 10^6 \exp\left(-\frac{2.0\ ev}{kT}\right) \frac{\mu m}{h} \quad \text{for (111) Si}$$

which may be simplified to

$$J = \frac{DN_o}{x + D/K} \tag{7}$$

If n is taken as the number of molecules of oxidant incorporated into unit volume of oxide

$$\frac{dx}{dt} = \frac{J}{n} + \frac{DN_o}{n\,(x + D/k)} \tag{8}$$

This may be solved by setting $x = o$ at $t = o$

$$(x + \frac{D}{k})\ dx = \frac{DN_o\ dt}{n} \tag{9}$$

and

$$\frac{x^2}{2} + \frac{D}{k} = \frac{DN_o t}{n} \tag{10}$$

or

$$x^2 + \frac{2Dx}{k} = \frac{2DN_o}{n}\ t \tag{11}$$

where x = oxide thickness

t = oxidation time

A,B= constants

This expression may be derived as follows. Considering the gradient of oxidant through the oxide layer shown schematically in Figure 6 allows the flux of oxidant to be written:

$$J \simeq \frac{D\,(N_o - N_i)}{x} \tag{2}$$

If it is assumed that the oxidant is consumed at the Si/SiO_2 interface by a first order reaction the rate may be expressed

$$R = k\,N_i \tag{3}$$

where k is the first order rate constant. At steady state R = J so that Eqn. 3 may be rearranged to

$$N_i = \frac{J}{k} \tag{4}$$

and substitution of (4) into (2) yields

$$J \simeq \frac{DN_o}{x} - \frac{DJ}{kx} \tag{5}$$

which may be rearranged to

$$J\left(1 + \frac{D}{kx}\right) = \frac{DN_o}{x} \tag{6}$$

Figure 28, whereas when the solubility is low the protrusions are less, Figure 28. As mentioned previously all protrusions become coated on their sides with Al_2O_3 and these protrusions generall extend completely through the alumina scale [27]. While numerous investigators have reported peg development of the type described above; other investigators have not seen such protrusions even though alloys with compositions thought to be appropriate for peg formation were oxidized.[29] Another noteworthy observation is that only one study [30] has reported internal oxidation of oxygen active elements whereby an internal subscale of discontinuous oxide particles were apparently formed. Whittle et al[30] internally oxidized hafnium in CoCrAl alloys by using a Rhines packs of Al_2O_3 and NiAl at 1200°C. In this study yttrium could not be internally oxidized. Based on the data available it can be proposed that internal oxidation of oxygen active elements from solution may not be possible for some alloys upon which Al_2O_3 scales are formed as external scales. For example the specimen shown in Figure 28b does not exhibit any features that show the yttrium in solution in the alloy is being oxidized internally. However, internal oxidation is evident in Figure 28a, but it is not a typical subscale structure and may be long stringers of oxide.

Thermodynamic data are not available to permit a rigorous calculation but the stability diagram presented in Figure 29 is the type that would be consistent with the proposal that the oxygen active elements in solution in the alloy will not be oxidized beneath an alumina scale.

If it is assumed that oxygen active elements cannot be oxidized beneath an alumina scale, the following mechanisms [31] is applicable to their oxidation. In the case of elements with low solubilities intermetallic compounds of the element are usually distributed throughout the alloy. As these alloys are oxidized the oxidation of the oxygen active elements is only possible in the vicinity of the intermetallic particles once a continuous layer of alumina is formed over the alloy. The oxidation process is described schematically in Figure 30. Upon exposure of the bare alloy to an oxygen containing environment, both aluminum and yttrium are oxidized, even yttrium in solution in the alloy, providing the oxygen pressure in the gas phase is high enough. For example exposure to air would certainly cause oxidation of the yttrium in solution, Figure 30a. As oxidation is continued the yttrium oxide particles will not grow unless an intermetallic particle is nearby to provide yttrium since the solubility of yttrium is so low. Hence after a short time the yttrium oxide formed by oxidation of yttrium in solution ceases to grow and becomes covered with the other oxides that continue to grow. In the case of alumina scales the growth of oxide is largely inward and so the yttrium oxide particles are confined to the outer part of the alumina scale adjacent to the alumina-gas interface.

It is important to note that the diffusion of oxygen in yttrium oxide is apparently high. At the base of the yttrium oxide particles the oxygen pressure may be significantly higher than at the alumina-alloy interface. However, if the flux of yttrium is not sufficient to permit yttrium oxide to be formed the tip of the particle will become coated

with alumina and its growth will stop. The data available show that yttrium is oxidized in the vicinity of the yttrium rich precipitates. It therefore is proposed that in the vicinity of the yttrium intermetallics a yttrium rich oxide phase is formed and it is incorporated into the inward growing Al_2O_3 as indicated in Figure 30b. In this case the yttrium oxide can grow at is base since there is sufficient yttrium delivered by the decomposition of the intermetallic particles. The sides of the protrusion soon become coated with Al_2O_3 for the same reasons that oxide particles formed by oxidation of yttrium in solution stop growing.. Consequently protrusions of yttrium oxide extend into the alloy at points where intermetallic particles existed in the alloy. It is important to note that protrusions will continue to grow only so long as a sufficient flux of yttrium is delivered to the protrusion tip. If this condition is not satisified, the tip will become separated from the alloy by a layer of Al_2O_3 and it will cease to grow at indicated in Figure 30b.

There are a number of characteristics of this model which are consistent with the literature. No protrusions will be formed if no intermetallic particles extend to the alloy surface prior to oxidation since a stringer of yttrium rich oxide extending through the alumina scale is a necessity for protrusion growth. In the case of alloys containing elements with higher solubilities, such as hafnium, the initial oxygen active oxides will be able to continue to grow due to the high flux of hafnium Figure 30c. It should be noted that these conditions can be significantly changed when carbon or nitrogen is present in the alloy to cause formation of carbides or nitrides. For such cases the solubility of the oxygen active elements will be significantly reduced and

protrusion formation will be possible only near carbide or nitride precipitates for reasons discussed previously for the yttrium rich intermetallic precipitates.

The model which has been developed is reasonably consistent with most of the existing data. It clearly shows how the distribution of intermetallic particles plays a critical role in the distribution of oxygen active element oxide pegs. It also illustrates how elements such as carbon and nitrogen can influence oxide protrusion development via reaction with the oxygen active elements.

The Effects of Oxygen Active Elements on Alumina Adherence

The effect of yttrium concentration on the adherence of alumina scales to Ni-20Cr-10Al allows has been studied. Concentrations over the range 0.03 to 1.2% yttrium have been studied. The alloy with a concentration of 1.2% had relatively poor adherence since oxide scale spalling occured in the vicinity of the large oxide pegs which formed on this alloy. Douglass [31] has also observed adverse effects from large oxide pegs. Optimum effects on oxide scale adhesion were obtained for 0.071% ytrrium. This concentration is just above the solubility limit for ytrrium in NiCrAl.[32] Very few pegs formed on this alloy. A number of the mechanisms used to account for the effects of oxygen active elements on oxide scale adhesion can be used to attempt to account for these results. At present the data in Table I that indicates a high bond strength for Al_2O_3 formed on this alloy is believed to offer a rather reasonable explanation.

Two hafnium concentrations in NiCrAl alloys, 0.27 and 0.98, have been studied. The data obtained shows that the alumina adhesion is

better on the alloy with 0.98 Hf than on the ally with 0.27. Furthermore the adherence of the alumina on the NiCrAl-0.071Y was better than on either of the Hf-containing alloys. It is believed that the 0.071Y is more effective in improving the adherence of alumina since it can establish better chemical bonding at the oxide-alloy interface than Hf. The fact that Hf caused improved adhesion as its concentration was increased, whereas Y exhibited better effects at 0.071 than 1.2 suggests that mechanical pegging may be important. Since Hf has higher solubilities in these alloys than Y, the hafnium protrusions are more numerous than the yttrium induced protrusions but of a significantly smaller size. Hence, the Hf pegs may not cause the stress concentration as the larger Y pegs do but rather mechanically key the oxide to the alloy.

Studies are being continued on determing the concentrations of oxygen active elements at which optimum adherence is developed. Furthermore the oxygen active element used and the base alloy are also significant factors to be considered.

The available results indicated that in examining the effects of oxygen active elements chemical bonding of the oxide to the alloy must be considered. However, it is also important to emphasize that the results are also consistent with the oxygen active elements affecting oxide scale adhesion by a number of different mechanisms, for example, chemical bonding, mechanical keying, as well as others.

CONCLUDING REMARKS

The investigation has emphasized the development of coatings beyond the state-of-the-art MCrAlY systems. It has been found that

the only oxides which can be used as barriers to effectively inhibit oxidation are Al_2O_3, Cr_2O_3 and SiO_2. Silica scales have been found to afford protection to alloys comparable to Al_2O_3 with potentially even better oxidation resistance. Acoustic emission techniques have been shown to provide an improved means to study oxide scale adhesion. Finally the type, concentration, and base alloy composition have been shown to be significant factors that determine the adhesion of alumina scales to alloy substrates.

During the fifth year of this program work will concentrate upon: (1) Conclusively documenting the properties of silica scales as barriers to resist oxidation. (2) Optimizing the acoustic emission method for characterizing the damage in oxide scales. (3) Defining the types and concentrations of oxygen active elements that are most appropriate for use in improving the adherence of oxide scales on MCrAl alloys.

REFERENCES

1. G.H. Meier and F.S. Pettit, "Fundamental Research Directed to Advanced High Temperature Coating Systems Beyond the Current State-Of-The-Art Systems," Third Annual Report, University of Pittsburgh, AFOSR, Contract No. 80-0089.

2. A. Ashary, G.H. Meier, and F.S. Pettit, "Acoustic Emission Study of Oxide Cracking", pp 105-119, High Temperature Protective Coatings, S.C. Singhal, editor, The Metallurgical Society, Warrendale, PA. 1983.

3. F.S. Pettit, "Oxidation of Nickel-Aluminum Alloys at Temperatures Between 900-1200°C Trans. AIME, 239, 1296 (1967).

4. G.C. Wood and F.S. Stott, The Development and Growth of Protective -Al_2-0_3 Scales on Alloys", in High Temperature Corrosion, R.A. Rapp, ed., NACE 1983, p. 227.

5. B.E. Deal and A.S. Grove, J. Appl. Phys., 36, 3770 (1965).

6. B.E. Deal, J. Electrochem. Soc., 125, 5765 (1978).

7. E. Rochet, B. Agins, and S. Rigo, J. Electrochem. Soc., 131, 914 (1984).

8. F.A. Kroger, "Defects and Transport in $Si0_2$, Al_20_3 and Cr_20_3", in High Temperature Corrosion, R.A. Rapp, ed. NACE, 1983, p. 89.

9. A.G. Revesy and H.A. Schaeffer, J. Electrochem. Soc., 129, 357 (1982).

10. E.A. Irene, J. Electrochem. Soc., 129, 413 (1982).

11. E.A. Irene, J. Appl. Phys., 54 5416 (1983).

12. J.M. Gibson and D.W. Dong, J. Electrochem. Soc., 127, 2722 (1980).

13. S.M. Hu, J. Appl. Phys. 55, 4095 (1984).

14. D.R. Wolters, J. Electrochem Soc., 127, 2075 (1980).

15. A. Fargeix and G. Ghibaudo, J. Appl. Phys, 56, 589 (1984).

16. R.B. Marcus and T.T. Sheng, J. Electochem. Soc., 129, 1278 (1982).

17. Wagner, C.J. Appl. Phys. 29, 1295, 1958.

18. Wagner, C. Corros, Sci., 5, 751, 1965.

19. Gulbransen, E.A., Andrew, K,F. and Brassart, F.A., J. Electrochem. Soc., 113, 834, 1966.

20. J.W. Hinze, W.C. Tupp, and H.C. Graham "Active Oxidation Phenomena in Silicon and Silicon-Based Materials", in Metal-Slag, Gas Reactions and Processes, Z.A. Foroulis and W.W. Smeltzer eds, The Electrochem Soc., 1975, p. 391.

21. L.H. Keys, "The Oxidation of Silicon Carbide", in Properties of High Temperature Alloys, A.A. Foroulis and F.S. Pettit, eds., The Electrochem. Soc., 1976, p. 681.

22. S.C. Singhal, "Oxidation of Silicon-Based Structural Ceramics", in Properties of High Temperature Alloys, p. 697, Z.A. Foroulis and F.S. Pettit, editors, The Electrochem Soc. 1976.

23. H.W. Grunling and R. Bauer, Thin Solid Films, 95, 3 (1982).

24. J.L. Cocking, L.D. Palmer, N.A. Burley, and G.R. Johnston, "High Temperature Oxidation of Alpha Nickel-Silicon", to be published in Oxidation of Metals.

25. J.W. Kerr and G. Simkovich, "Hot Corrosion Studies on Nickel-Based Alloys Containing Silicon" in Properties of High Temperature Alloys, Z.A. Foroulis and F.S. Pettit, eds., The Electrochem Soc., 1976, p. 576.

26. G.M. Kim, J. Caola and G.H. Meier, unpublished research on Martin Marietta Subcontract 19X-43369C.

27. C.S. Giggins and F.S. Pettit, "Oxide Scale Adherence Mechanisms and the Effects of Yttrium, Oxide Particles and Externally Applied Loads on the Oxidation of NiCrAl and CoCrAl Alloys" performed at Pratt and Whitney Aircraft for the Aerospace Research Laboratories, Wright-Patterson AFB, Ohio; Final Report, June, 1972; ARL TR 75-0234.28

28. H. Hindam and D.P. Whittle, J. Electrochem. Soc.,129, 1147 (1982).

29. A.S. Kahn, C.E. Lowell and C.A. Barrett, J. Electrochem. Soc., 127, 670 (1980).

30. I.M. Allam, D.P. Whittle, and J. Stringer, Oxid, of Metals, 13, 381 (1979).

31. J. Caola, F.S. Pettit, G.H. Meier, to be published.

32. J.D. Kuenzly and D.L. Douglass, Oxid. Metals, 8, 285 (1968)10.

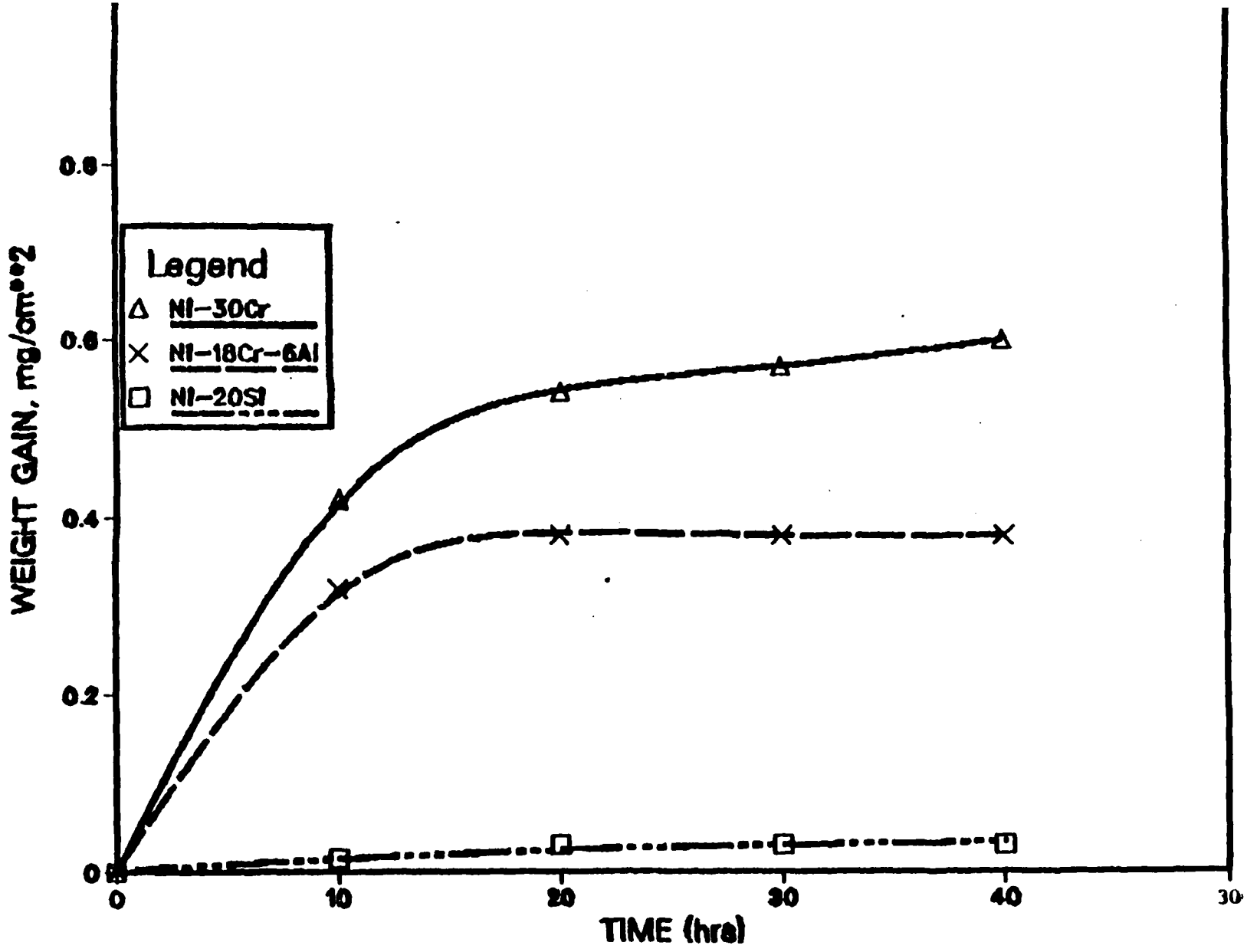

Figure 1. Comparison of weight change data for alloys which depend upon Cr_2O_3(Ni-30Cr), Al_2O_3(Ni-18Cr-6Al) and silica (Ni-20Si) scales for protection (1000°C in air).

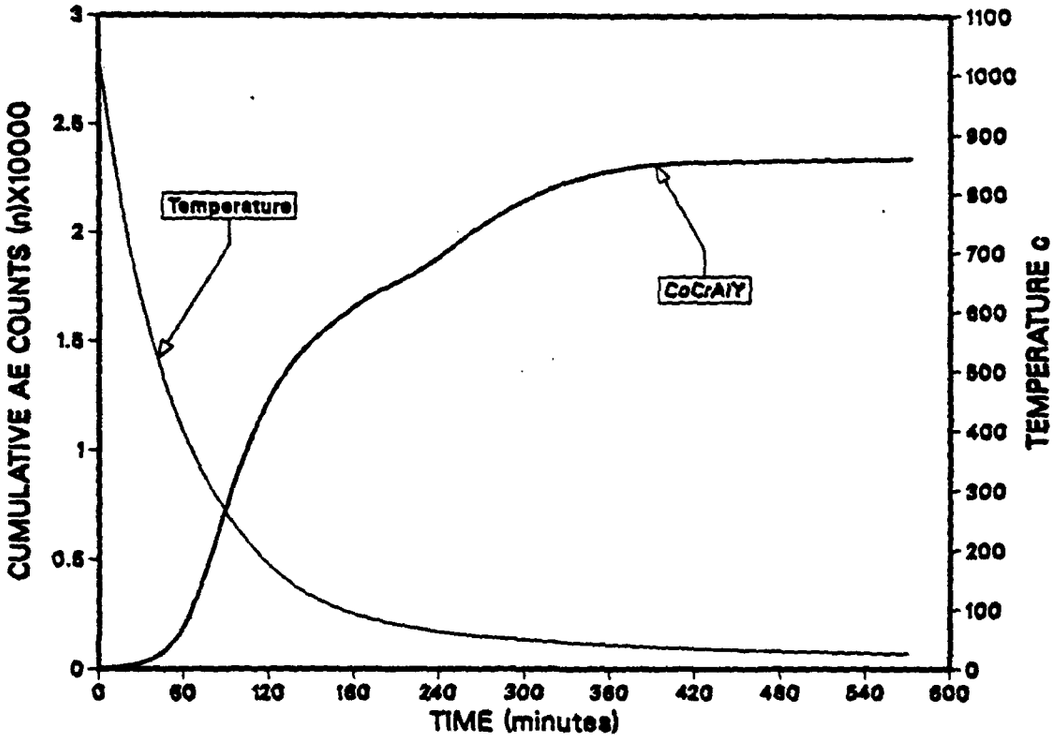

Figure 2. Acoustic emission counts detected during cooling of a Co-22Cr-11Al-0.5Y alloy after 24 hr. oxidation in air at 1050°C.

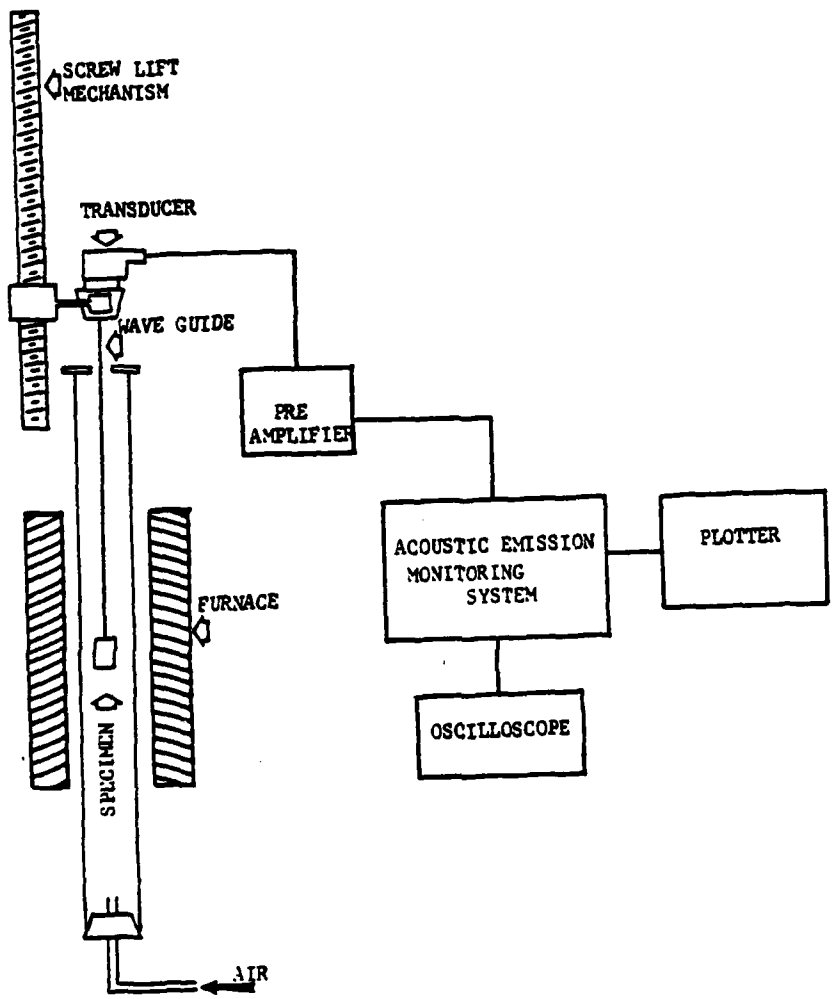

Figure 3. Schematic Diagram of acoustic emission apparatus used for studying high-temperature oxidation.

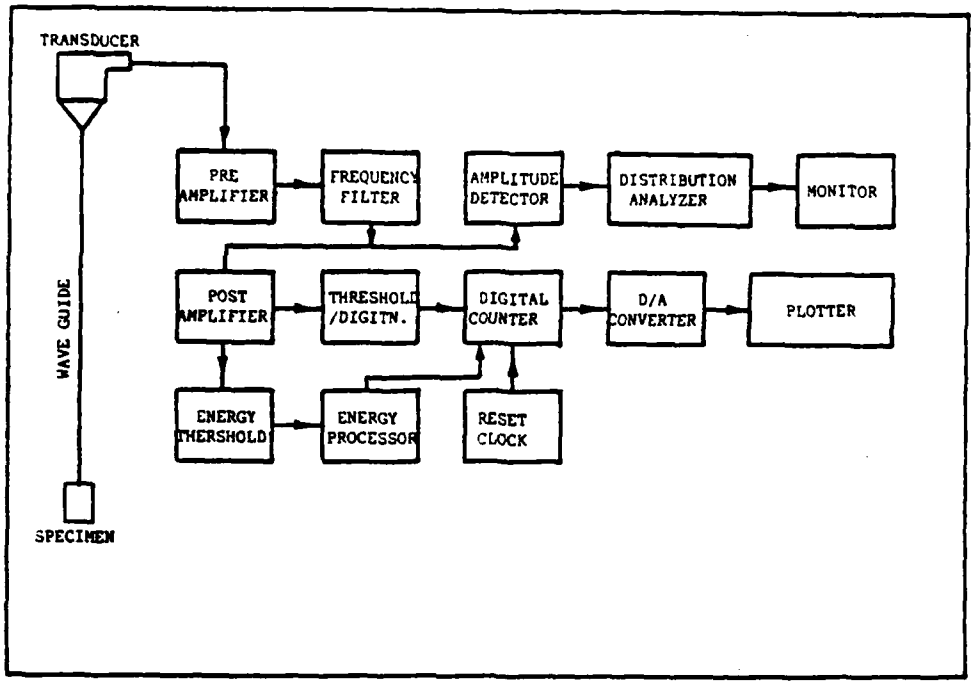

Figure 4. Function block diagram of acoustic emission detection system.

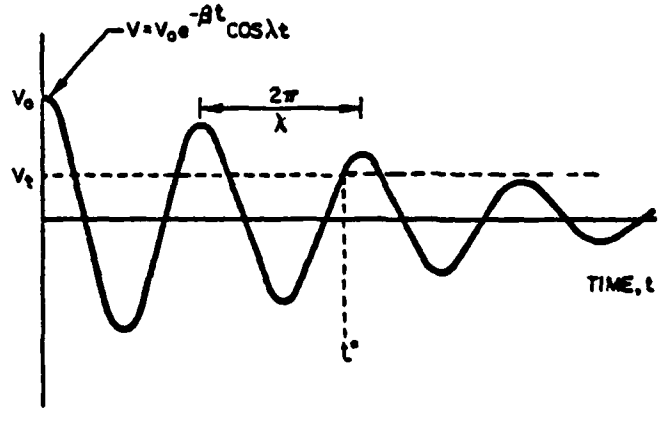

Figure 5. Schematic diagram of "ringing down" of an acoustic emission signal.

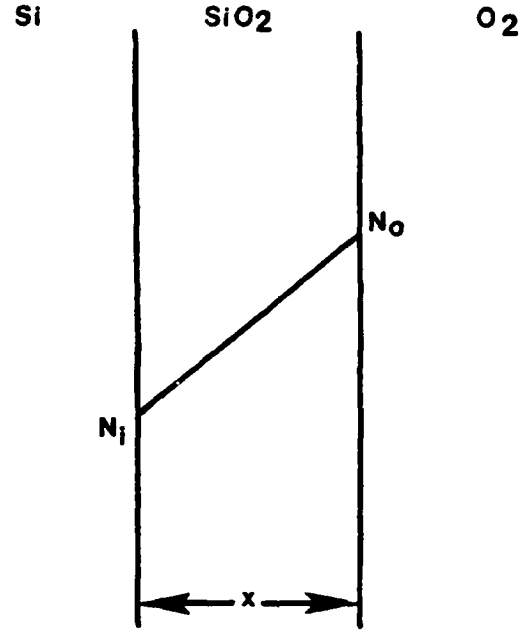

Figure 6. Schematic gradient of oxygen across an oxide layer on silicon.

Amplitude Distribution Analysis
NiCrAl-0.071Y

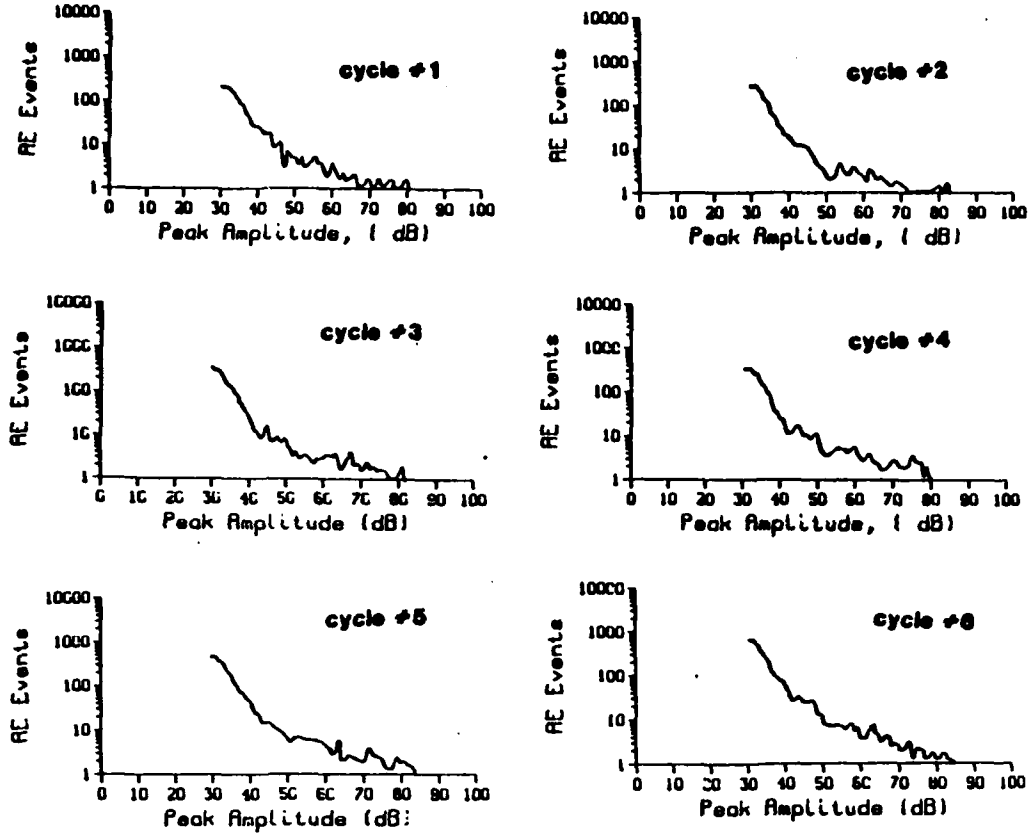

Figure 20. Amplitude distribution obtained on cooling after 24 hours of oxidation at 1100°C in air.

Amplitude Distribution Analysis
CoCrAl-1.0Hf

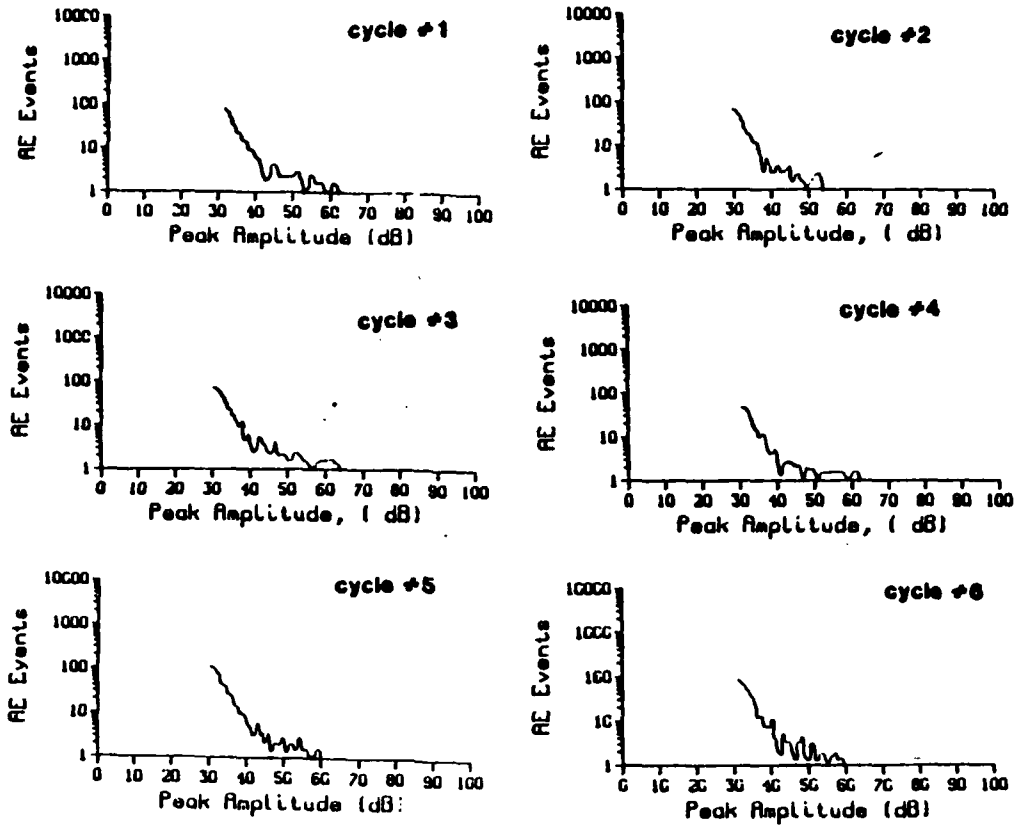

Figure 19. Amplitude distribution obtained on cooling after 24 hours of oxidation at 1100°C in air.

Amplitude Distribution Analysis
CoCrAl-0.066Y

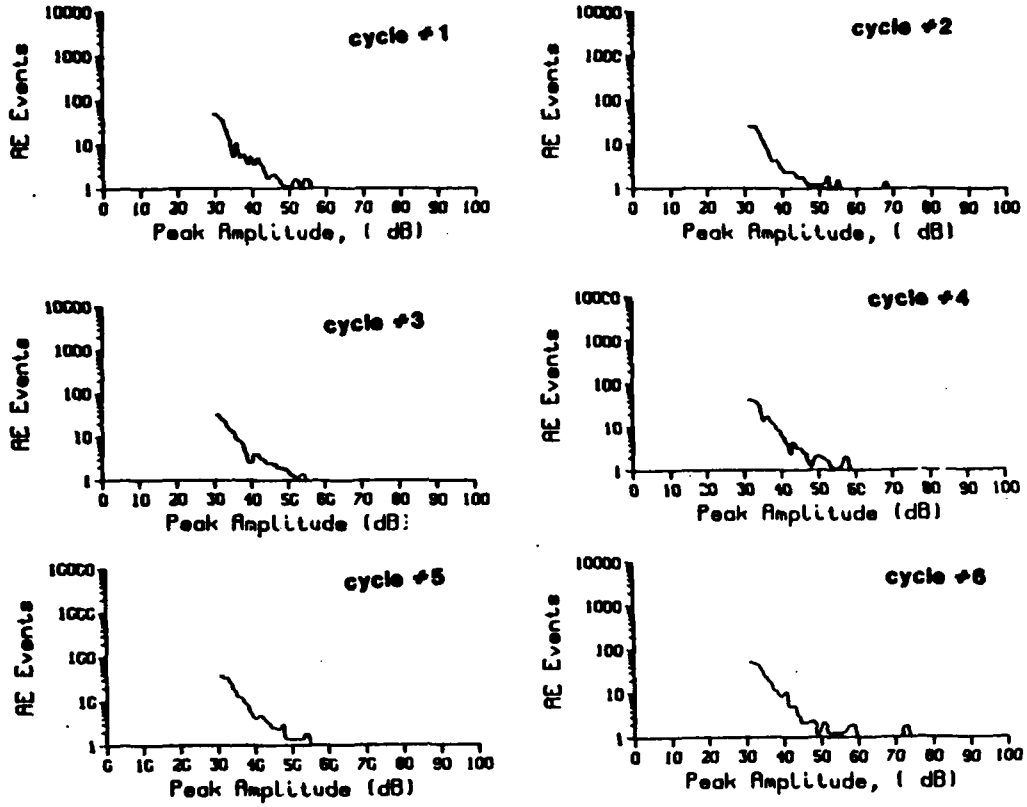

Figure 18. Amplitude distribution obtained on cooling after 24 hours of oxidation at 1100°C in air.

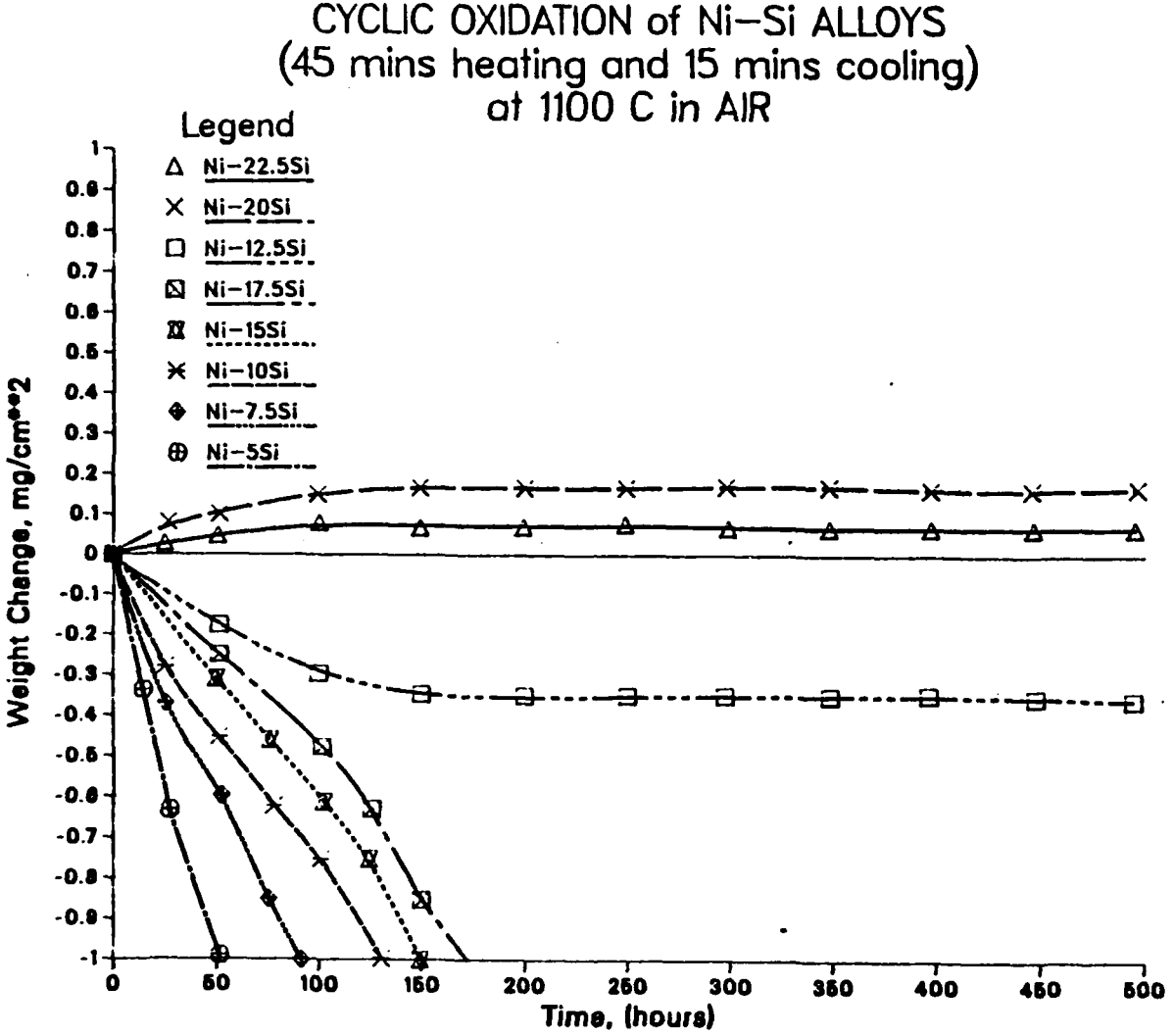

Figure 17. Cyclic oxidation data for alloys studied in the current program

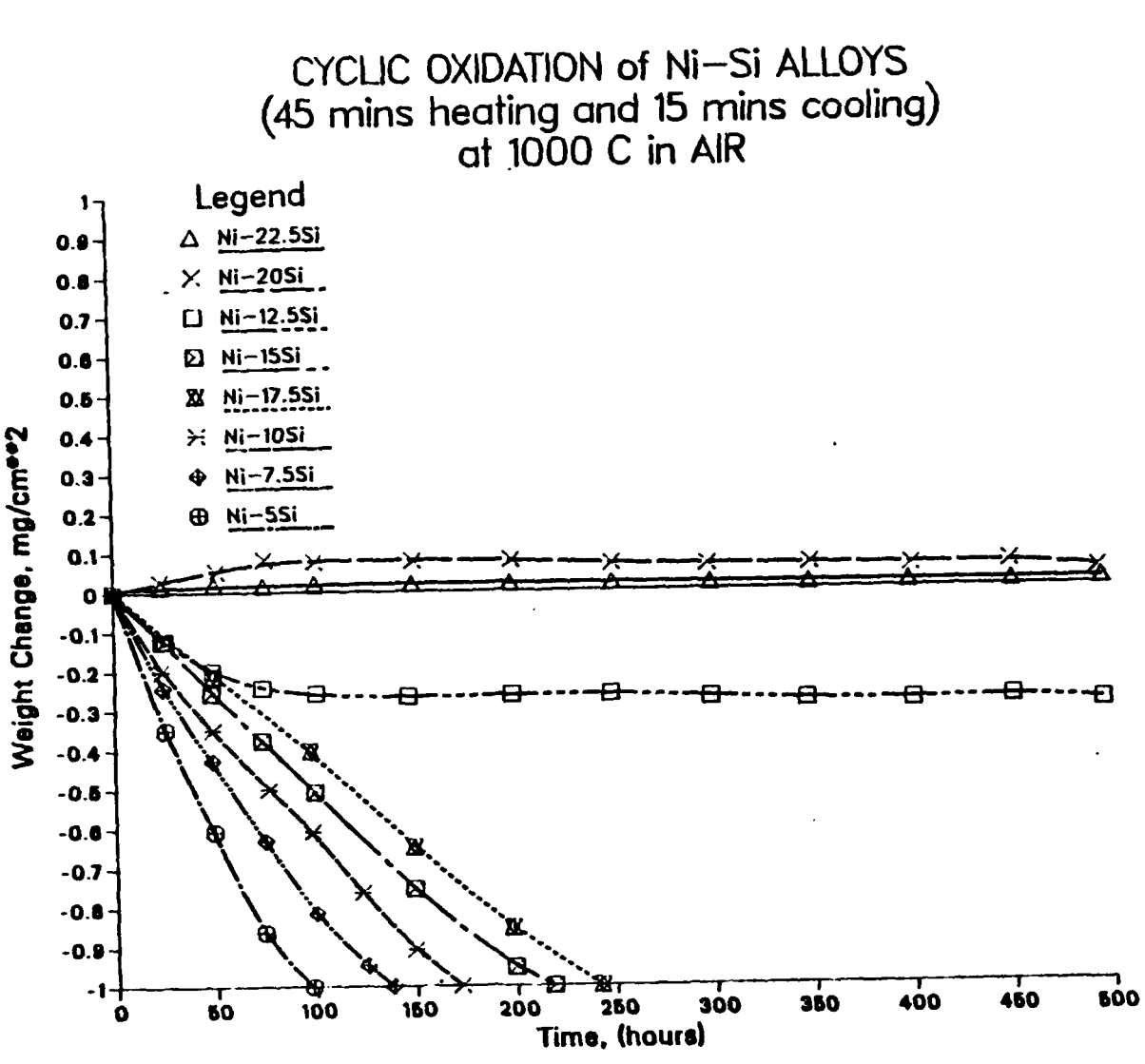

Figure 16. Cyclic oxidation data for alloys studied in the current program.

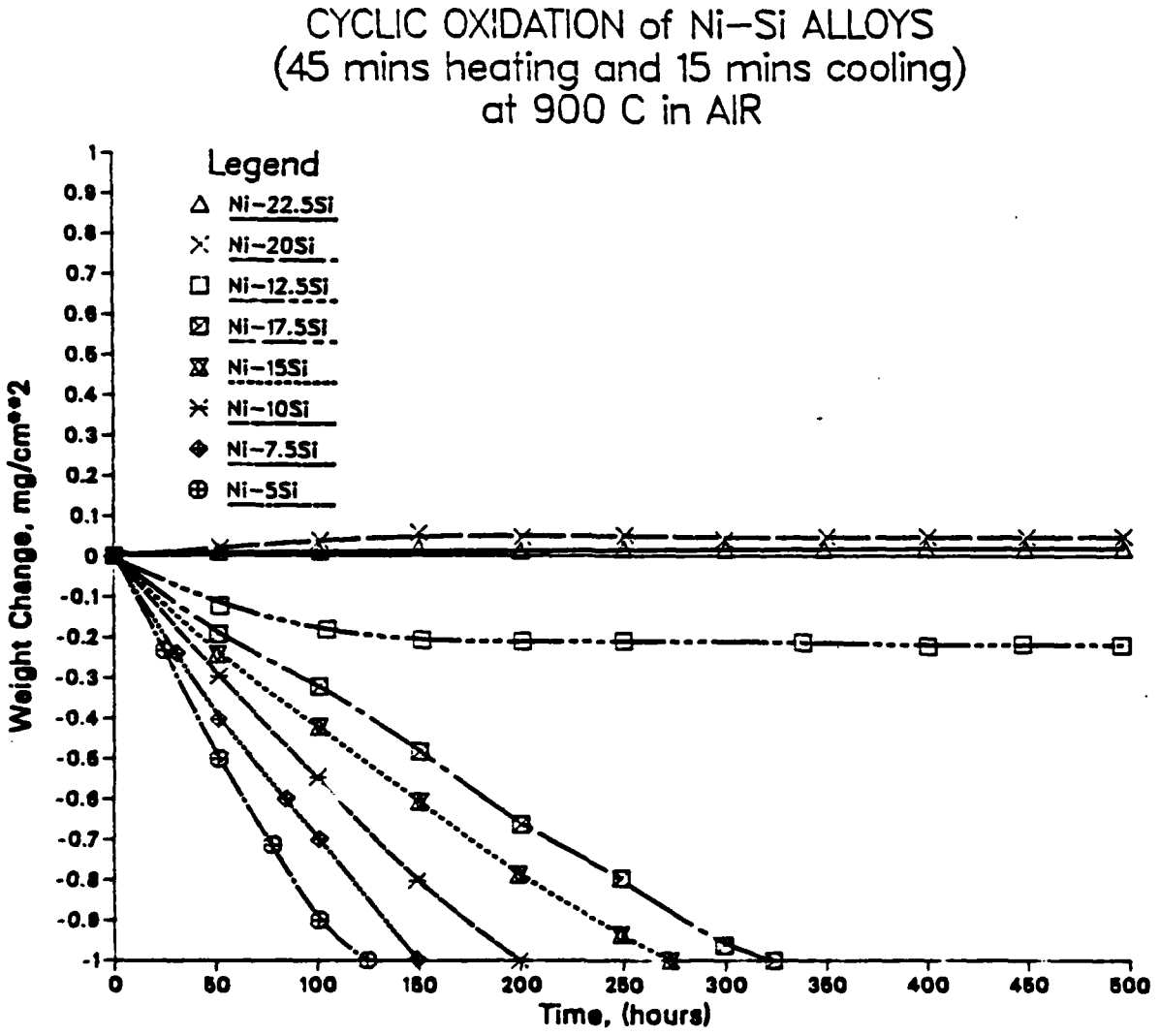

Figure 15. Cyclic oxidation data for alloys studied in the current program.

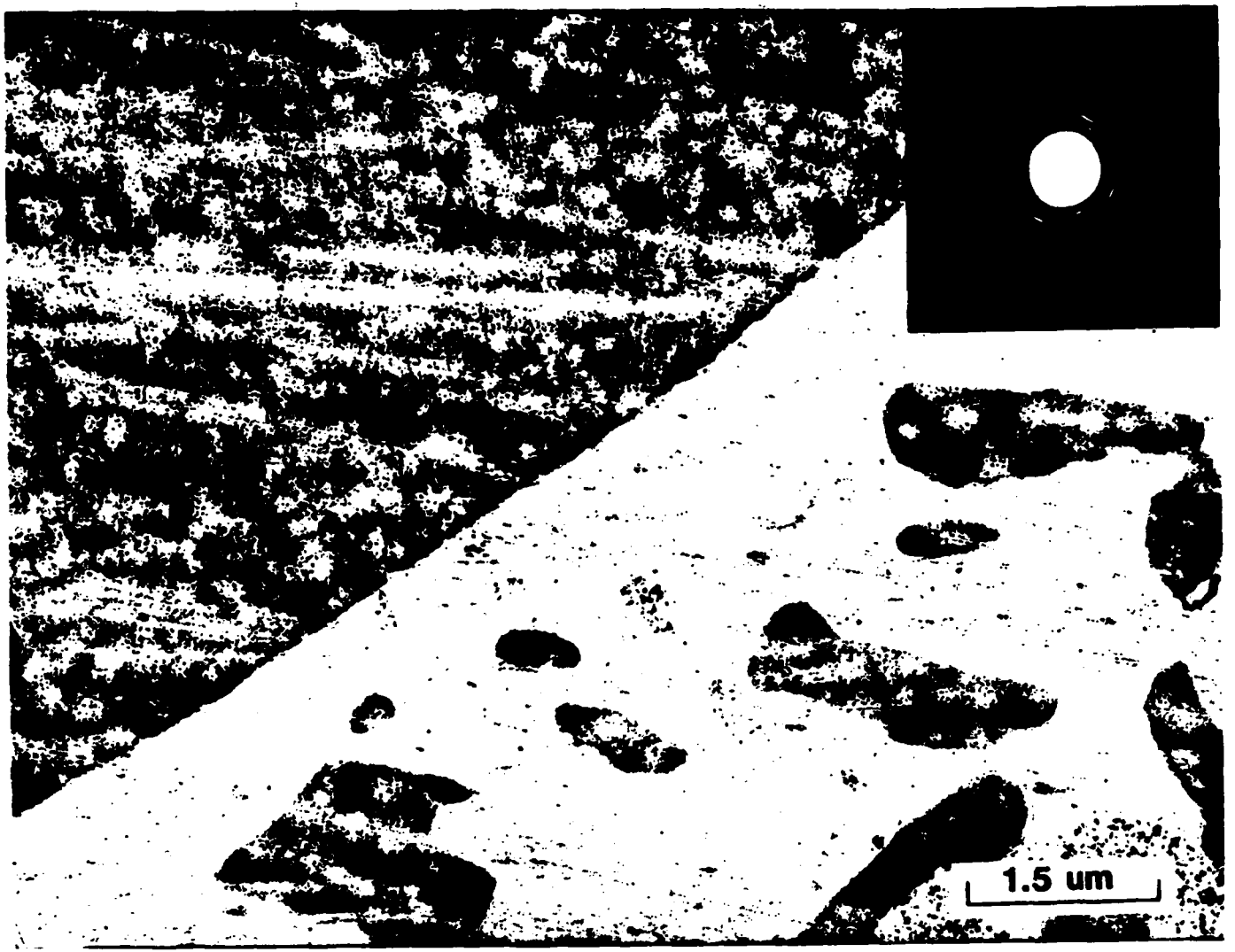

Ni–20Si, Oxidized at 950 C for 1 hr.

Figure 14. Transmission micrograph of oxide stripped from two phase region shown in Figure 13.

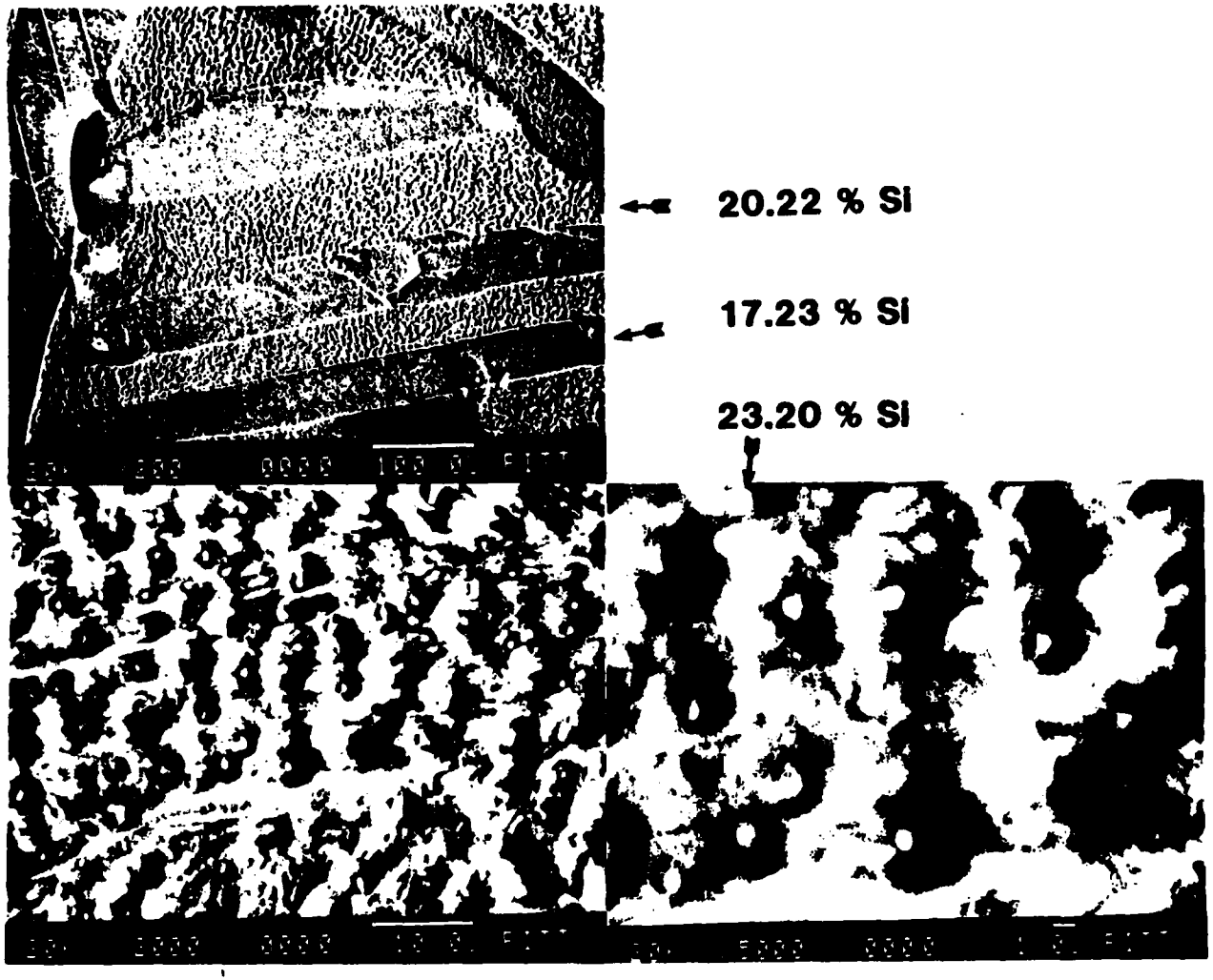

Ni–20Si, Homogenized at 1100 C.

Figure 13. Scanning micrographs of homogenized Ni-20Si alloy.

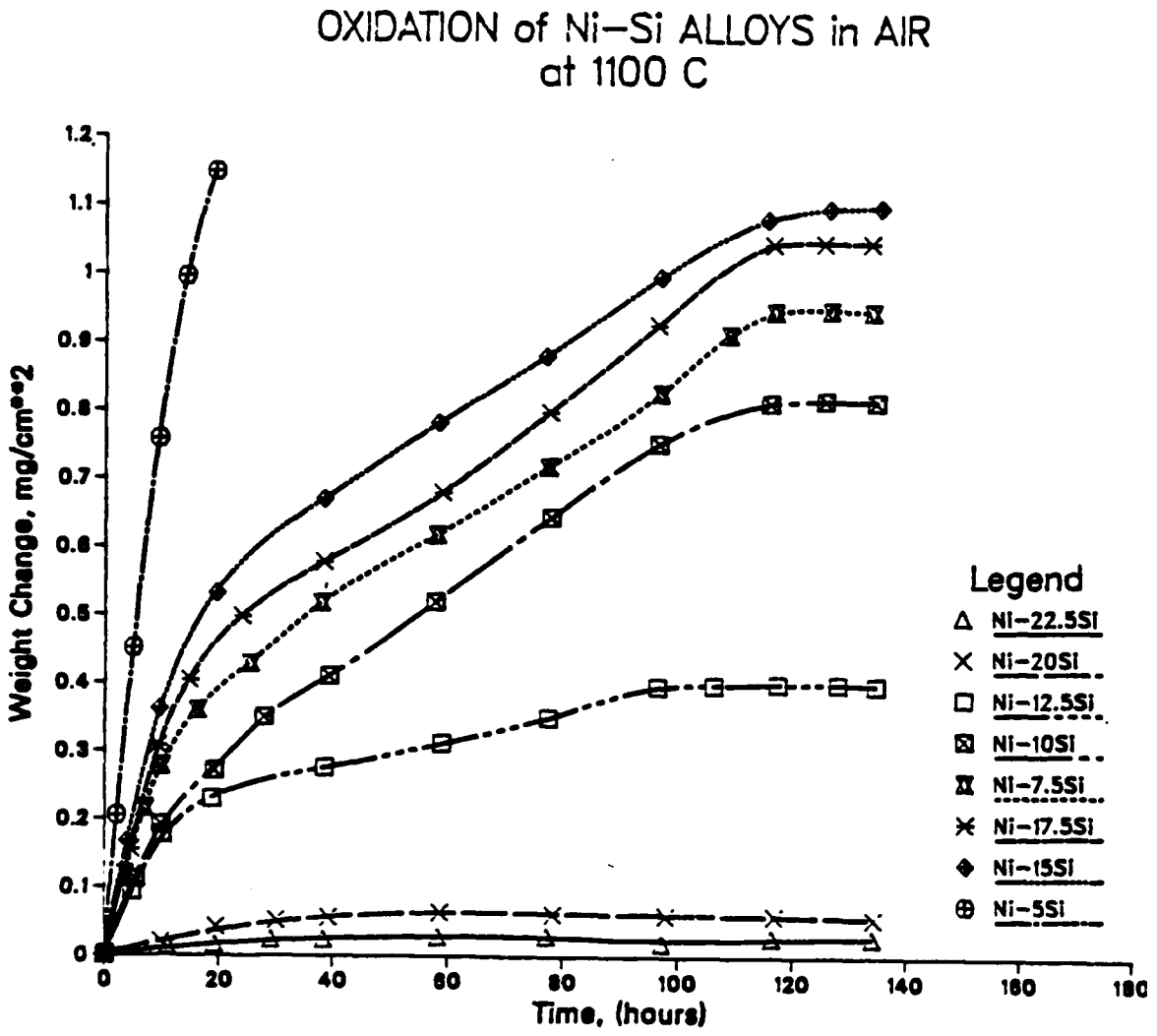

Figure 12. Isothermal oxidation data obtained for alloys studied in current program.

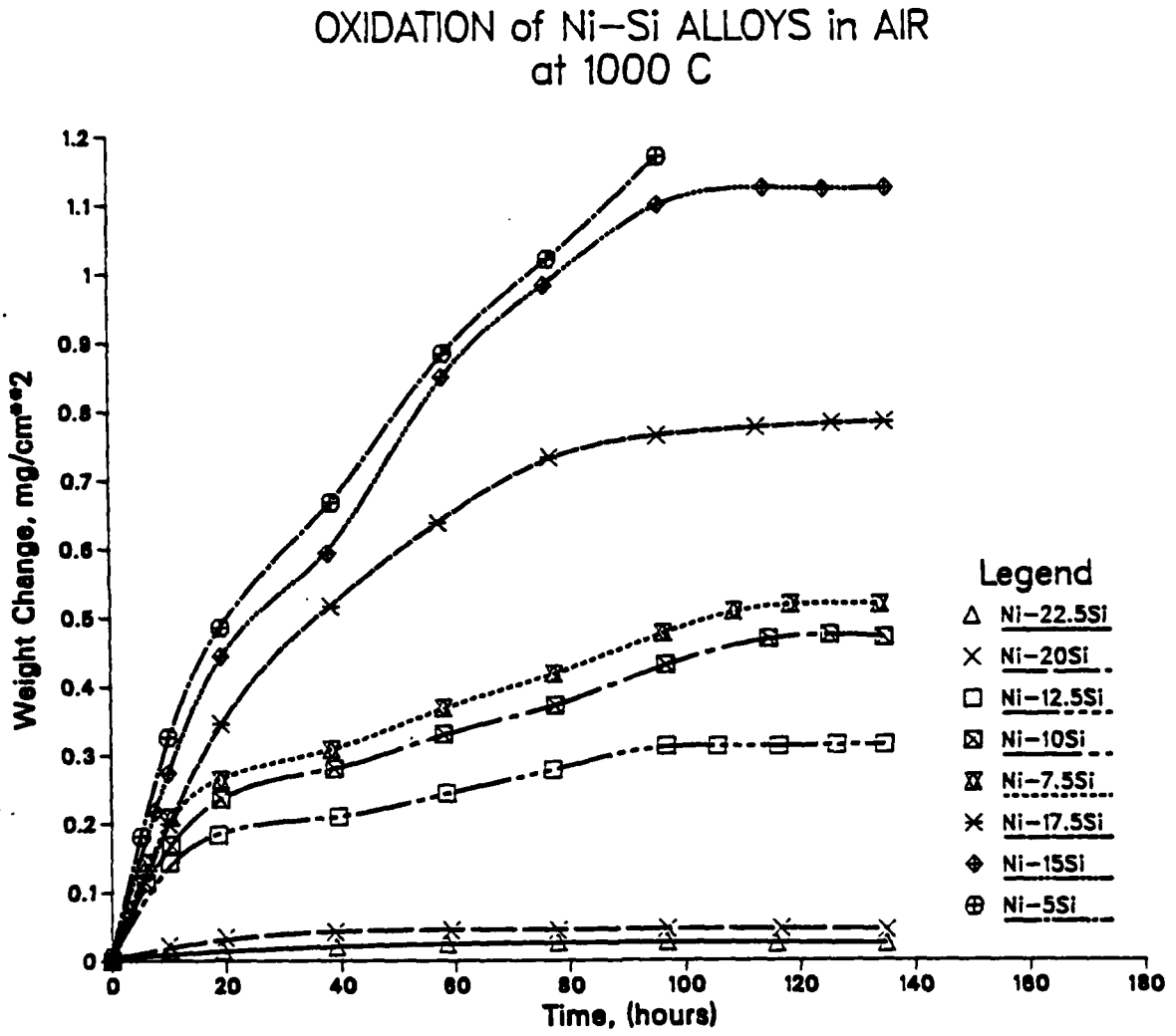

Figure 11. Isothermal oxidation data obtained for alloys studied in current program.

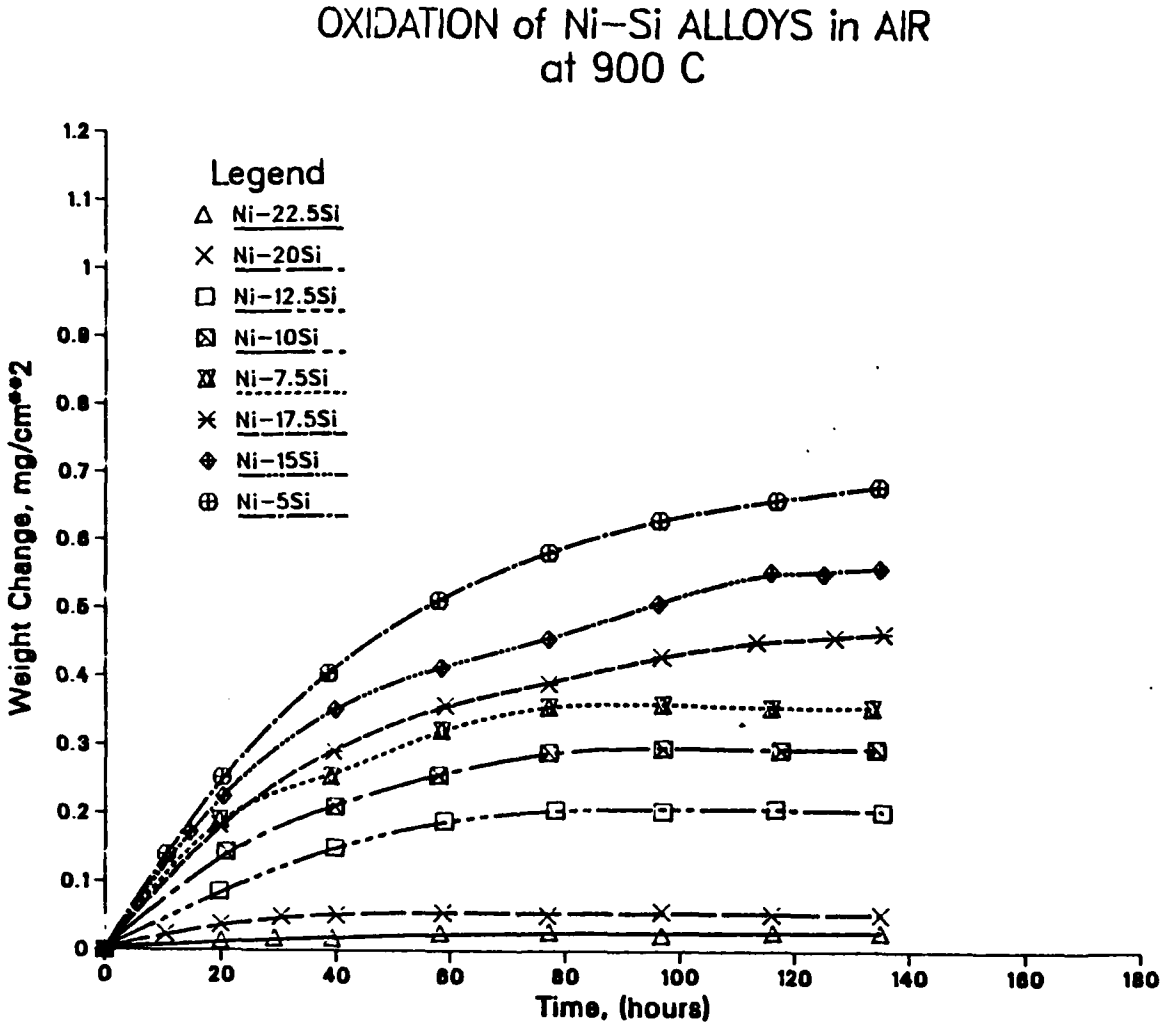

Figure 10. Isothermal oxidation data obtained for alloys studied in current program.

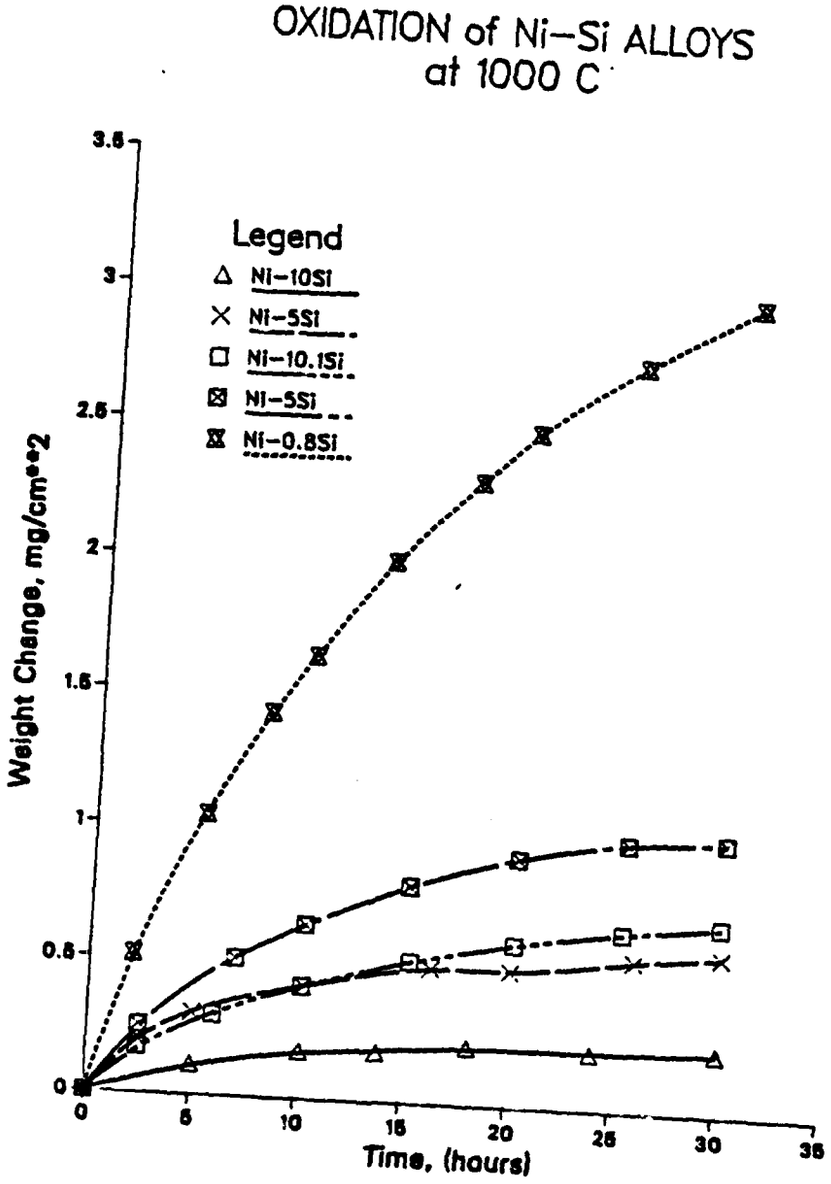

Figure 9. Weight change versus time data for oxidation of nickel-silicon alloys at 1000° in air.

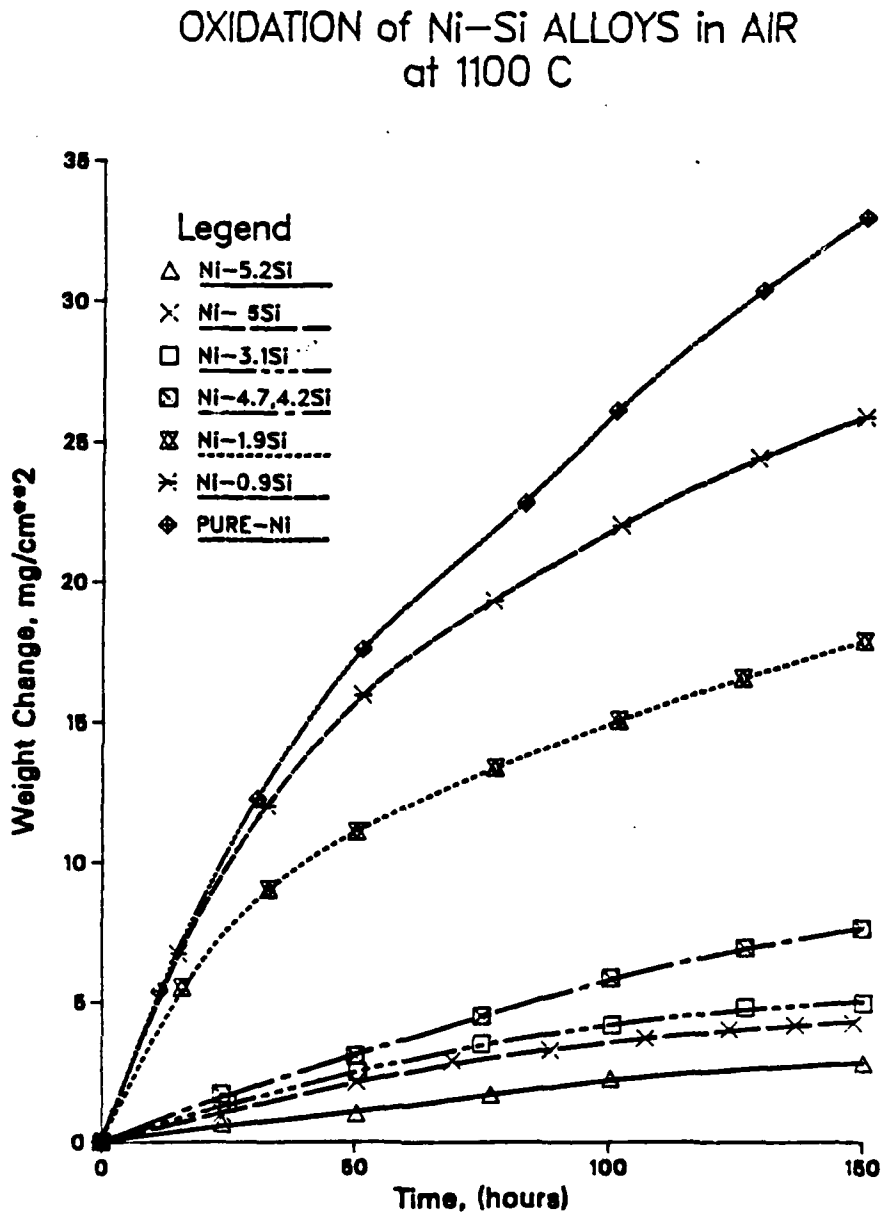

Figure 8. Weight change versus time data for the isothermal oxidation of some nickel-silicon alloys at 1100°C in air.

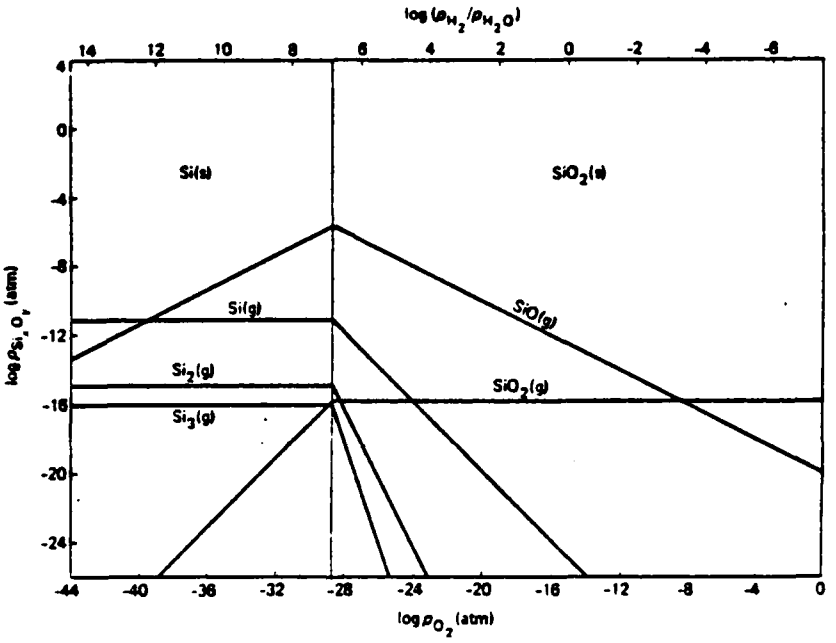

Figure 7. Si-O system volatile species at 1250 K

Amplitude Distribution Analysis

NiCrAl-1.2Y

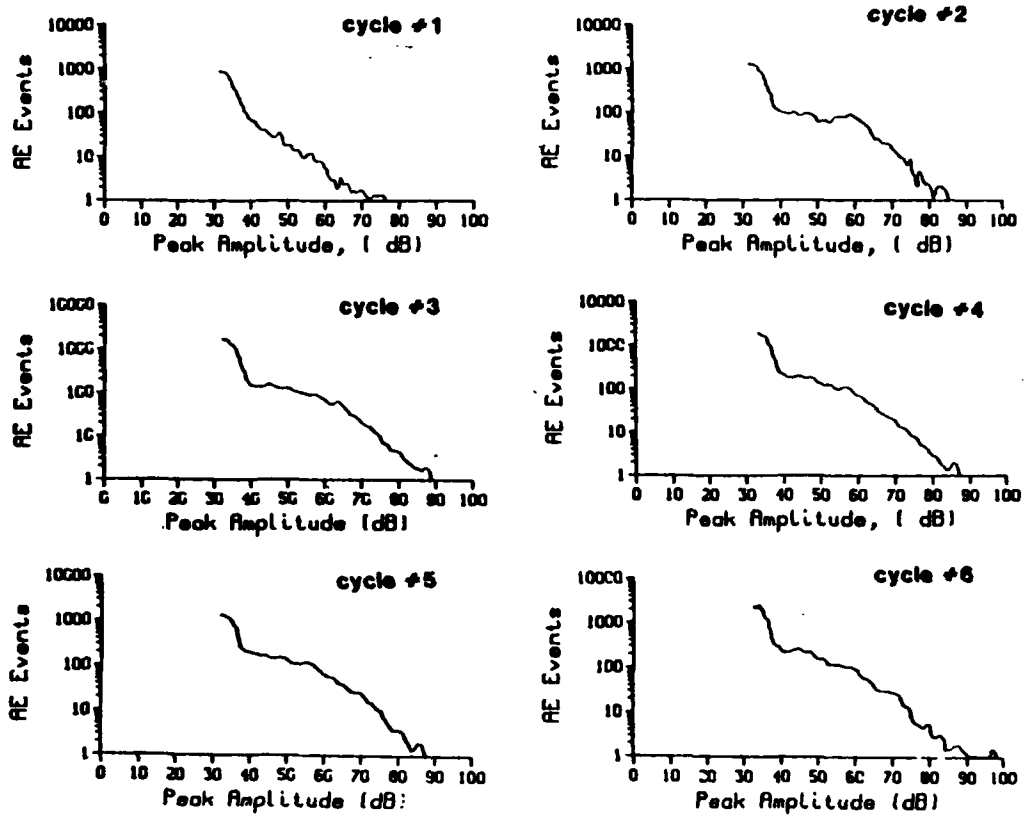

Figure 21. Amplitude distribution obtained on cooling after 24 hours of oxidation at 1100°C in air.

Amplitude Distribution Analysis
NiCrAl-0.98Hf

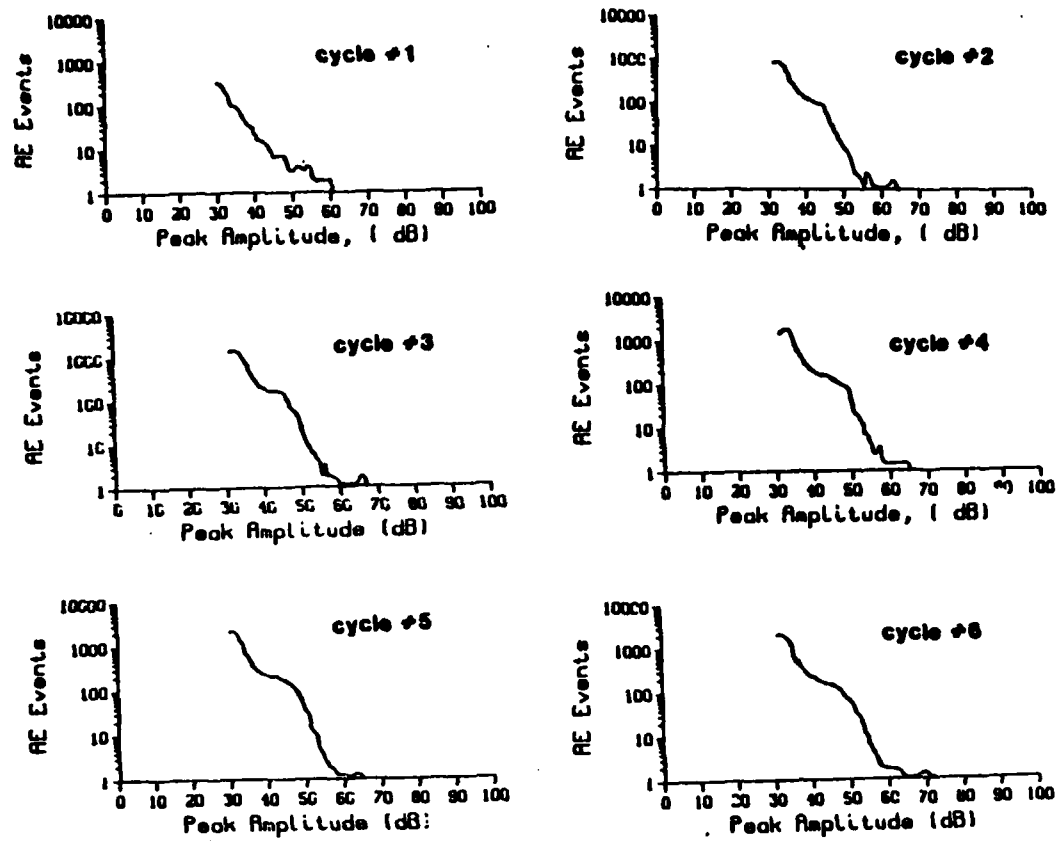

Figure 22. Amplitude distribution obtained on cooling after 24 hours of oxidation at 1100°C in air.

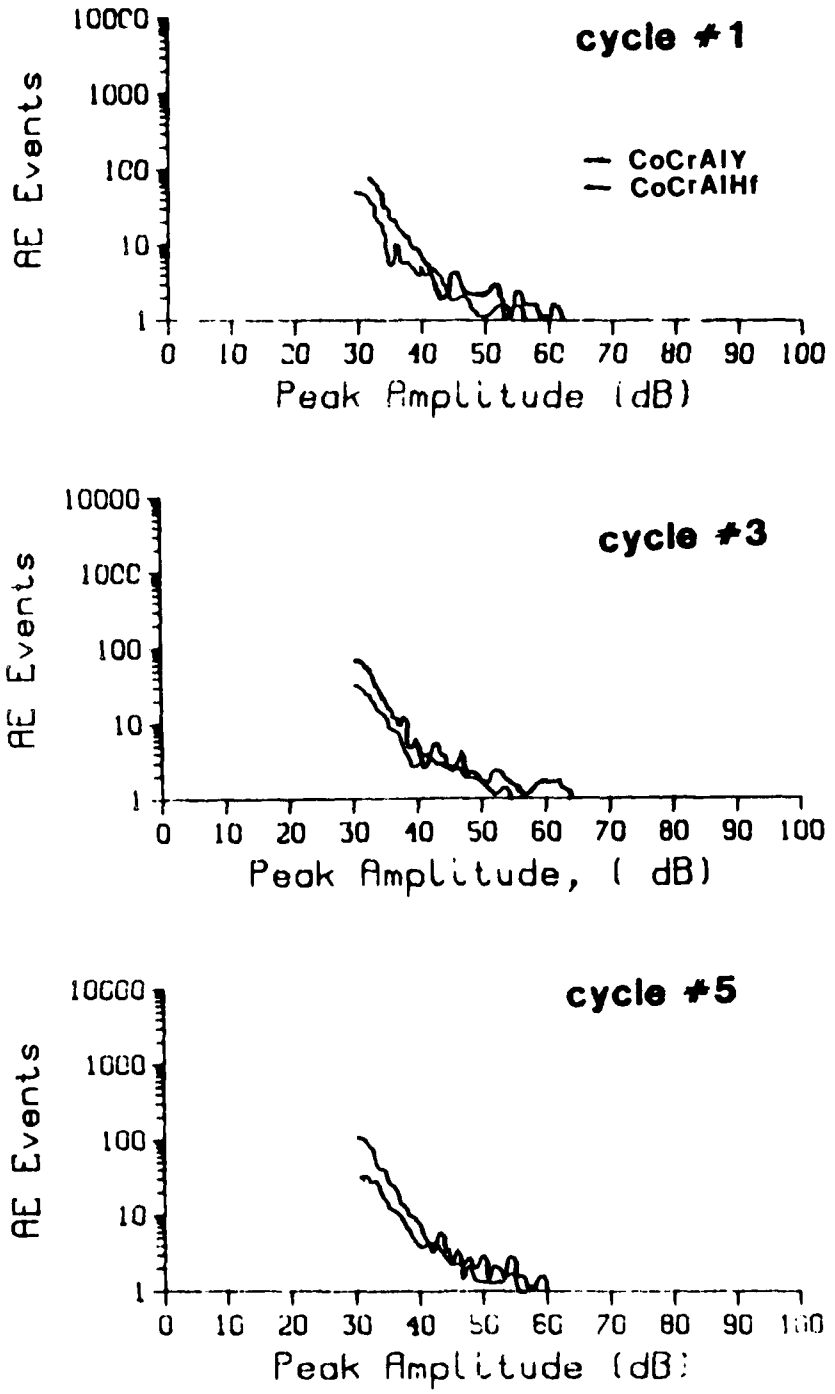

Figure 23. Comparison of amplitude distributions for CoCrAl-.066Y and CoCrAl-1.0Hf.

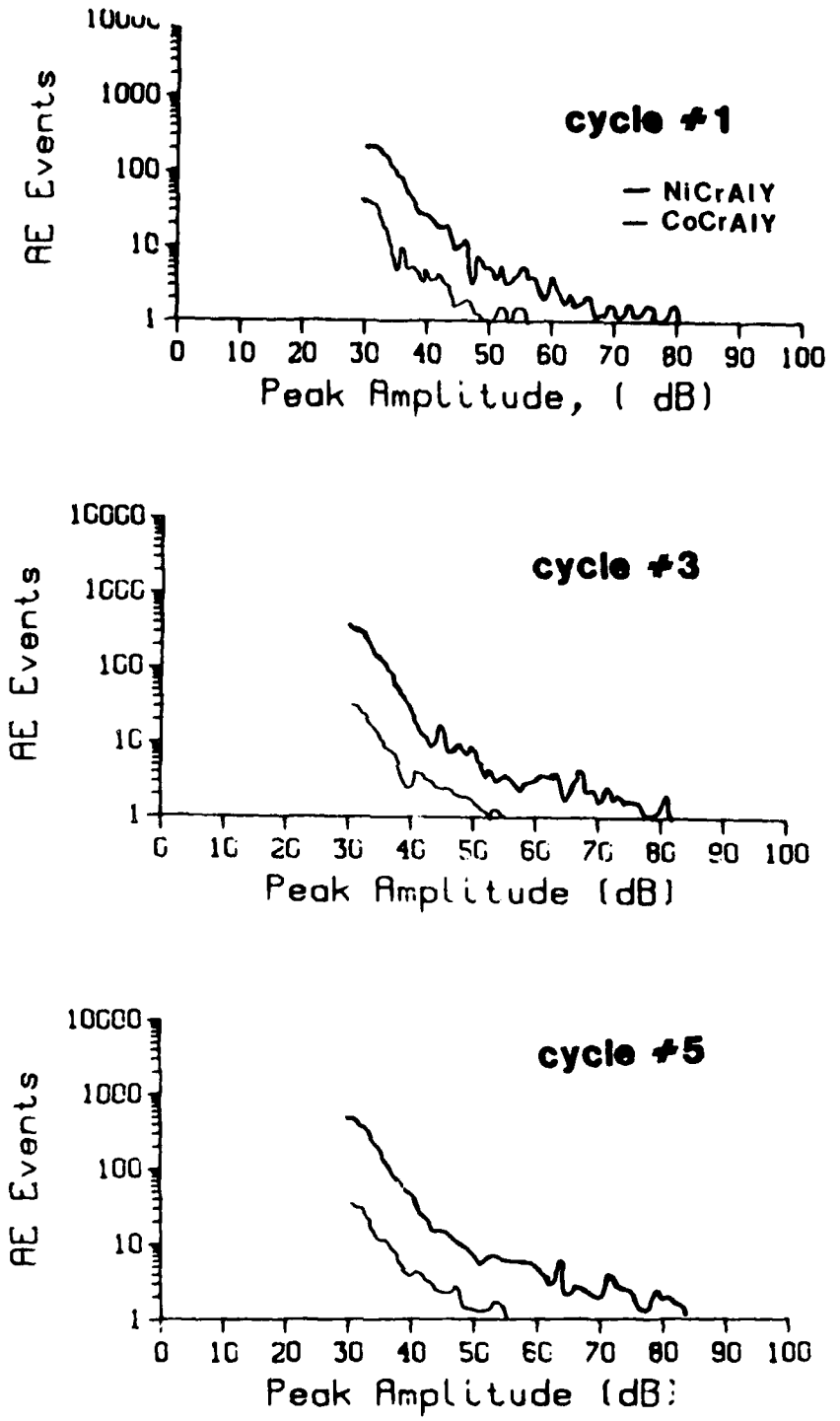

Figure 24. Comparison of amplitude distributions for CoCrAl -.066Y and NiCrAl - .071Y.

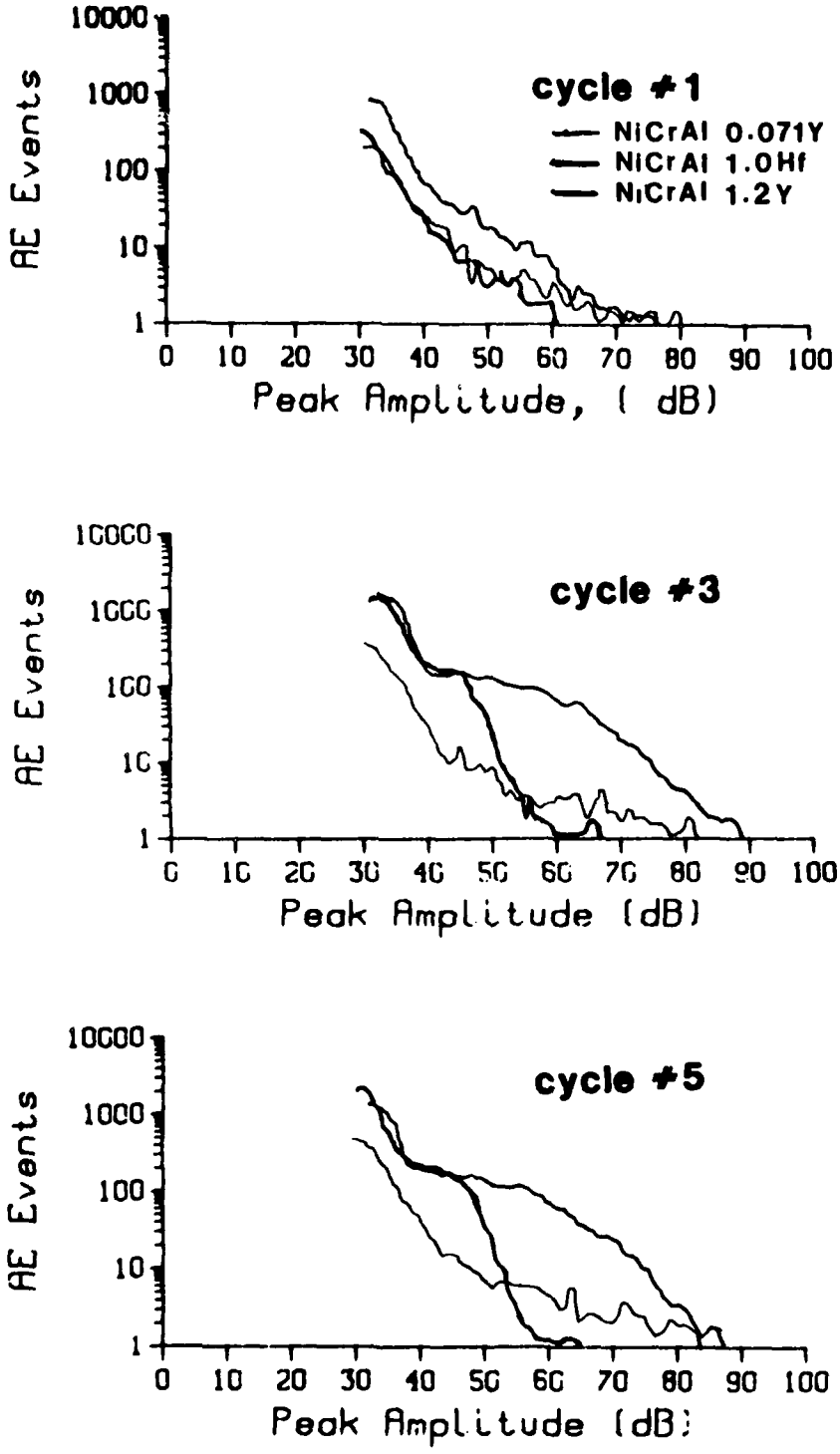

Figure 25. Comparison of amplitude distirubtions for NiCrAl -1.2Y, NiCrAl - 1Hf and NiCrAl -.071Y.

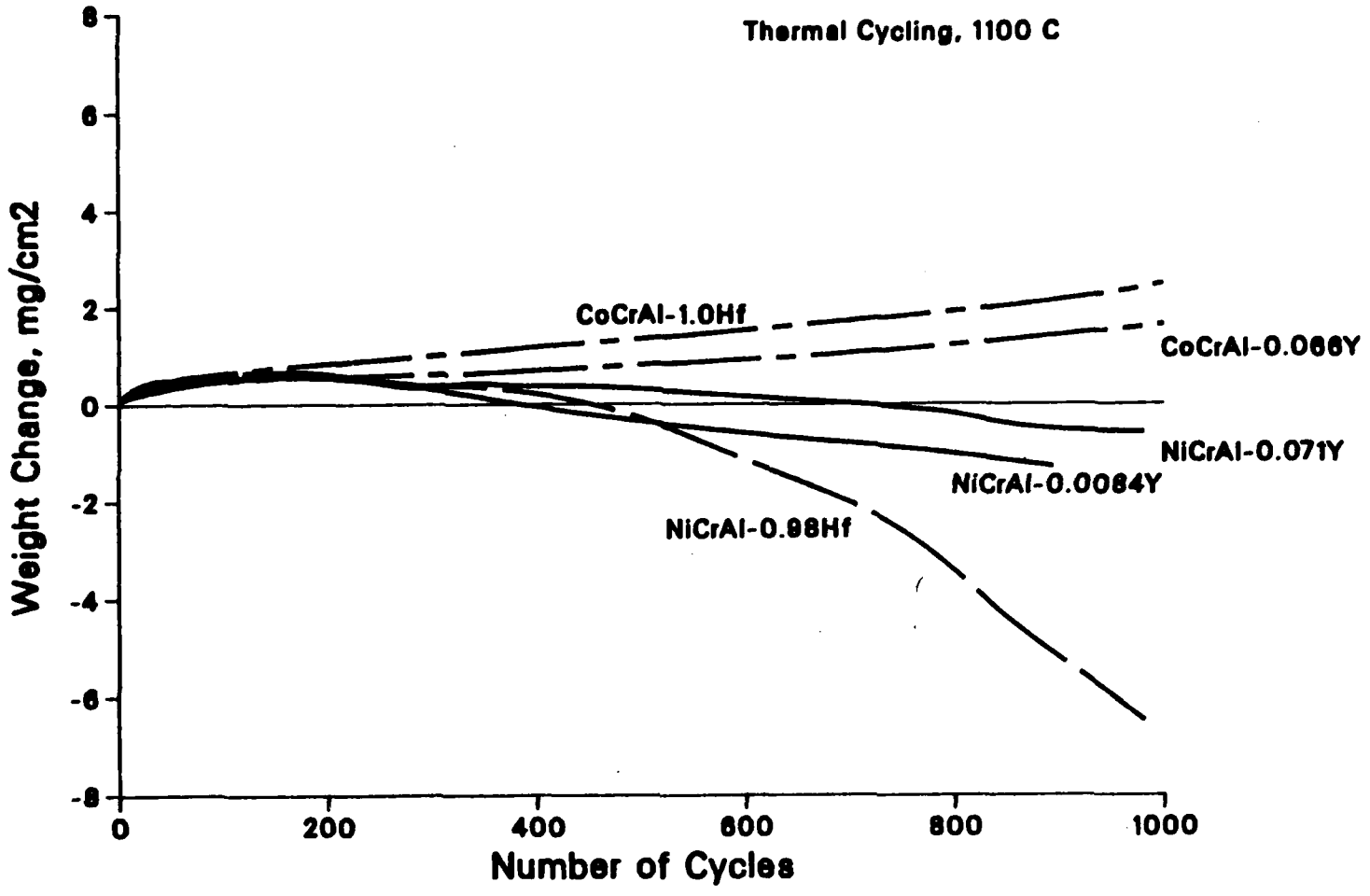

Figure 26. Cyclic oxidation data (1 cycle to room temperature per hour) for alloys oxidized at 1100°C in air.

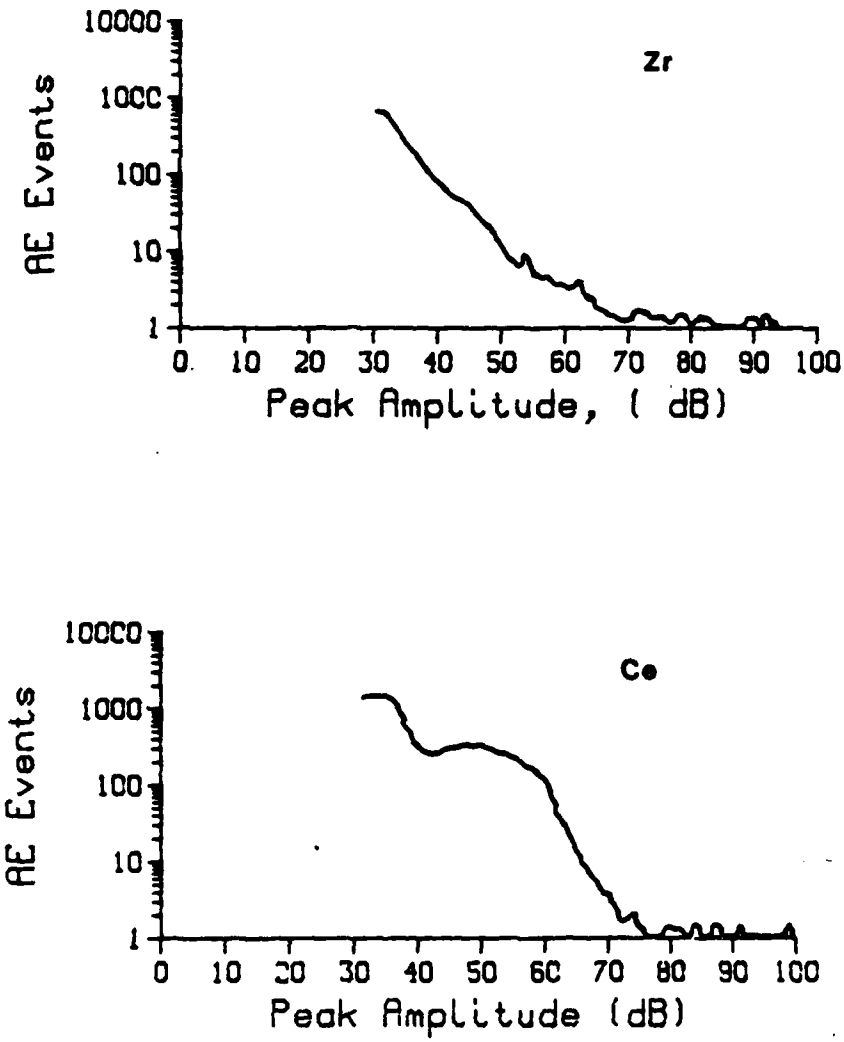

Figure 27. Preliminary data obtained for specimens of NiCrAlCe and NiCrAlzr alloys, the amplitude distributions were obtained upon cooling specimens after 24 hours of oxidation in air.

a

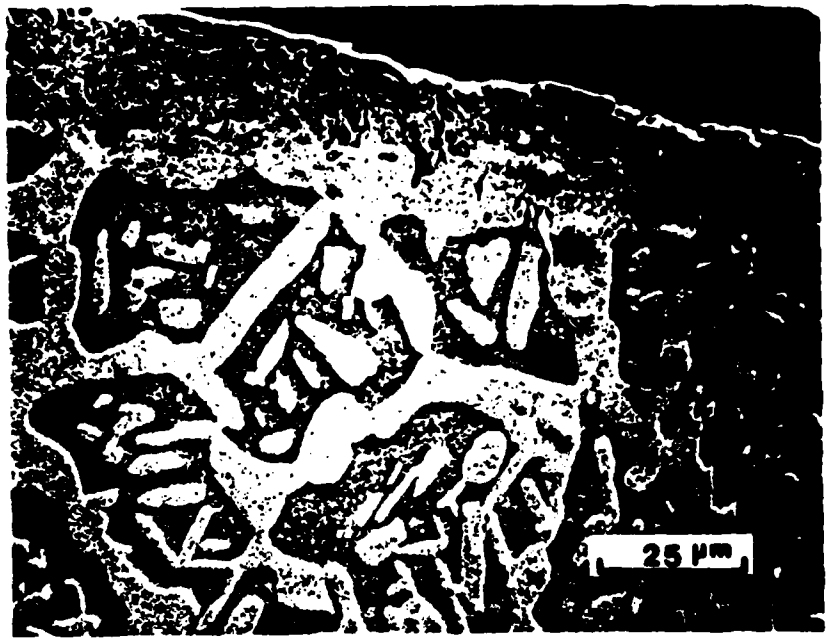

CoCrAlHf

b

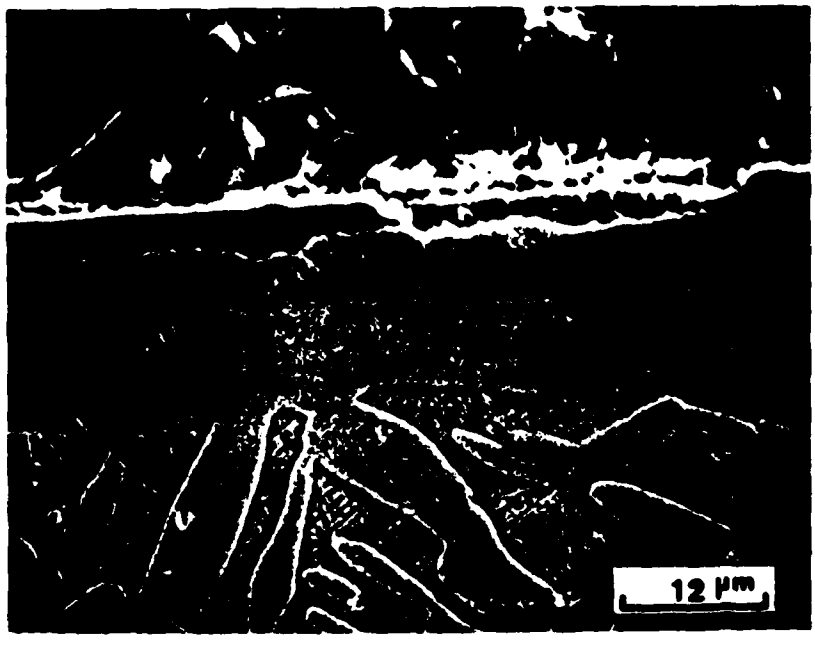

CoCrAlY

1000 hrs thermal cycling at 1050 C

Figure 28. Optical micrographs obtained for oxidation of CoCrAlHf (high solubility) and CoCrAl (low solubility) oxygen active elements.

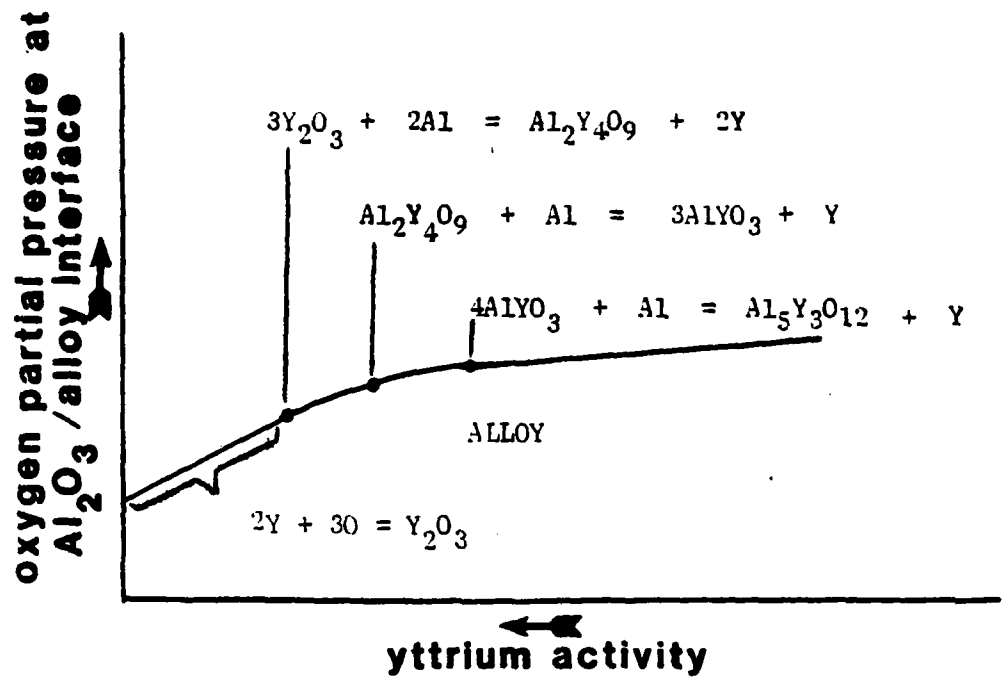

Figure 29. Quasi-stability diagrams for the formation of yttrium and yttrium-aluminum oxides beneath an AL_2O_3 scale on an MCrAl alloy.

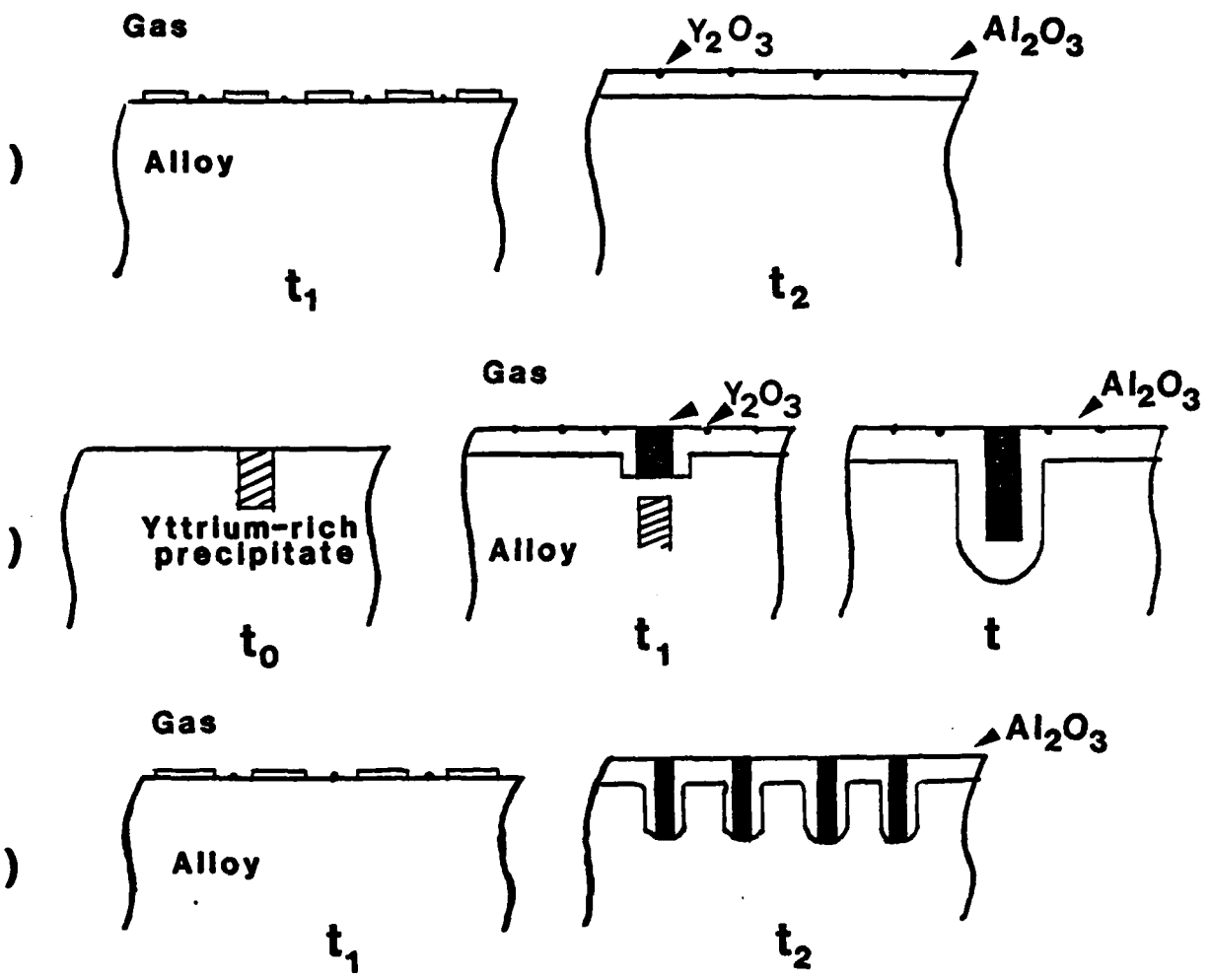

ɹure 30. Sketches to illustrate oxide scale and subscale development for: (a) an alumina former containing a low solubility oxygen active element in solution, (b) an alumina former with a low solubility oxygen active element at a concentration sufficient to form intermetallic precipitates, (c) an alumina former containing an oxygen active element with high solubility.

TABLE I

Energy Per Spalled Area Obtained Using
Acoustic Emission Counts and Spalled Areas

	Total Energy Counts	Spalled Area (cm)	Energy/Spalled Area (Counts/cm)
iCrAl	8.630×10^6	2.772	3.114×10^6
iCralY	0.988×10^6	0.019	5.116×10^7
iCrAlHf	1.152×10^6	0.018	6.141×10^7

END

FILMED

4-85

DTIC